Radiometric calibration and monitoring of NOAA AVHRR data for ISCCP

CHRISTOPHER L. BREST[†] and WILLIAM B. ROSSOW

NASA Goddard Space Flight Center, Institute for Space Studies,
2880 Broadway, New York, NY 10025, U.S.A.

(Received 22 May 1989; in final form 14 May 1990)

Abstract. This paper describes the methodology developed to monitor the radiometric calibration of NOAA AVHRR data and to normalize succeeding polar orbiters for the International Satellite Cloud Climatology Project (ISCCP). Results are presented for NOAA-7, -8, and -9 Channel 1 (visible) data and briefly for Channel 4 (thermal infrared) in an appendix. The successful normalization of NOAA-8 and NOAA-9 to NOAA-7 allows the ISCCP calibration standard to be maintained over time. A correction for the degradation of NOAA-9 data and an absolute calibration for the entire ISCCP dataset are presented.

1. Introduction

1.1. *Calibration of satellite data*

The necessity of accurate and comprehensive calibration of satellite radiometers to provide quantitative measurements for Earth studies is beginning to be realized (Robinove 1982, Price 1987, Slater *et al.* 1987). The recent increase in the use of satellite data for climate studies calls for the determination of physical parameters from the measured radiances and therefore for absolute calibrations that are known over long time periods. Moreover, plans to collect global satellite data over decadal periods to monitor changes in surface conditions (Price 1987) and in climate (NASA 1984) require a calibration standard that can be transferred from one satellite to another in a series.

Although most instruments undergo a thorough calibration prior to their launch on a satellite, there appears to be no predictable relationship between these pre-launch calibrations and the post-launch performance. Thus, comprehensive, well-documented post-launch calibrations are needed. Thermal infrared channels on most radiometers are calibrated with an on-board thermal source and a view of deep space and are thought to be well calibrated. Since the solar channels used for imaging on most operational satellites do not have on-board calibration capabilities, an Earth-target approach to calibration is the only method available.

High resolution sensors, such as Landsat MSS, have been calibrated using man-made surfaces (Lyon *et al.* 1975, Brest and Goward 1987), as well as natural surfaces (Ahern *et al.* 1977, Kowalik *et al.* 1982, Castle *et al.* 1984). Calibration of lower resolution sensors, like those used for monitoring the weather and climate, is limited to the use of larger natural targets. Examples are the calibration of: the METEOSAT visible channel by Koepke (1982) using ocean, savanna, pasture and snow, and by

[†] ST Systems Corp.

Kriebel (1981) using ocean, treeless vegetation and cloud, (2) the GOES and NOAA visible channels by Frouin and Gautier (1987) using White Sands (desert), and the NOAA visible channels by Staylor (1990) using the Libyan desert. However, even with the use of a good target, such as White Sands, problems are encountered, e.g. changes in the sand dunes and their shadows caused by the winds (Price 1987, Slater *et al.* 1987) and high water tables in some portions that cause variable soil moisture (Frouin and Gautier 1987, Slater *et al.* 1987). Desert vegetation can also vary seasonally and from year to year depending on rainfall (Whitlock *et al.* 1987). The number of these problems which are to be avoided determines the amount of effort and expense associated with a field campaign to obtain such calibration data (Price 1987); making such measurements routinely and for more than one target is usually not attempted. This limits results to two-point calibrations (target plus space) and to one or two measurements over the lifetime of a particular satellite.

Use of Earth surface targets to monitor the relative calibration of satellite instruments over long time periods introduces a number of other factors that cause diurnal and seasonal changes in the radiation from the target as seen by the satellite: variations in viewing and illumination geometry, changes in the atmosphere, navigation (Earth-location of the individual image pixels) errors in heterogeneous areas, changes in the surface characteristics (such as soil moisture and vegetation), and cloud variations. In addition, the effort required to repeat the field measurements many times for many sites usually prevents such programs from being carried out. This is despite well documented occurrences of significant calibration drifts over the life of some satellite radiometers. Examples are the Coastal Zone Color Scanner (CZCS), which experienced about a 25 per cent degradation in the 443 nm channel (Hovis *et al.* 1985), and Landsat 1 MSS, which suffered about a 25-32 per cent decrease in apparent reflectance values (Nelson 1985).

1.2. *ISCCP data and calibrations*

1.2.1. *ISCCP Stage B3 data*

The International Satellite Cloud Climatology Project (ISCCP), the first project of the World Climate Research Program, began its operational data collection in July 1983. The project is designed to take advantage of the global satellite coverage provided by current and planned operational weather satellites, both geostationary and polar orbiting. One objective is the collection of a uniform global radiance data set which can be analyzed to obtain a climatology of cloud properties to improve their parameterization in climate models (Schiffer and Rossow 1983). Data have been collected (to date) from the imaging radiometers on the NOAA polar orbiters (NOAA7, 8, 9, 10 and 11) and from the geostationary satellites, GOES (GOES-5, 6 and 7), METEOSAT (MET-2,3 and 4) and GMS (GMS-1, 2, 3 and 4). Such a satellite data set was collected for one year for the First GARP Global Experiment (FGGE), but the ISCCP data collection represents the first comprehensive, global, multi-year data collection.

The ISCCP Stage B3 data (Schiffer and Rossow 1985, Rossow *et al.* 1987) are the raw image radiances from all the satellites that have been reduced in volume, navigated, radiometrically normalized, and placed in a common format. Three different calibration tables are available to convert the digital count values to radiances. The first calibration table, nominal, represents the best initial information available for each satellite, often the pre-launch values. The second calibration table, normalized, represents the normalization of the geostationary satellites to the current polar orbiter,

and the normalization of succeeding polar orbiters to NOAA-7. Corrections for short-term changes or long-term drifts in the calibration are provided in the third ("absolute") calibration table. Normalization and calibration corrections are made only for the 0.6μm and 10-11μm wavelength channels that are common to all satellites; for the NOAA AVHRR, these are referred to as Channel 1 and Channel 4, respectively. The ISCCP Stage B3 version of AVHRR data are identical to the global area coverage (GAC) form, which has a nominal resolution of 4 km, except that they are truncated from 10 to 8 bits and are reduced by sampling the GAC pixels at a 24 km spacing.

These data form one of the two main products produced by ISCCP (Schiffer and Rossow 1985) and are archived at the ISCCP Central Archive (Satellite Data Services Division, NOAA/NESDIS, Washington, DC 20233).

1.2.2. *ISCCP radiometric calibration*

The information in this section is taken from Rossow *et al.* (1987).

Integer count values (CT_8 = 0 - 255, where the subscript 8 refers to 8 bit data) on ISCCP radiance data tapes represent the original radiances L (Wm^{-2} sr^{-1}), measured by the operational weather satellite imaging radiometers. These radiometers are narrowband, making measurements in limited ranges of the solar and thermal infrared spectra. In the short wavelength (solar) region of the spectrum, radiance can also be expressed as a (bidirectional) reflectance R by dividing L by the effective solar spectral irradiance E_o of the radiometers and the cosine of the solar zenith angle measured at the target: $R = \pi L/\mu_o E_o$. *Scaled radiance* is defined as $L^* = \pi L/E_o = \mu_o R$; it represents the fraction of energy measured by the radiometer assuming that the signal spectrum is the solar spectrum. High count values on B3 data tapes correspond to high radiances or reflectances. In the infrared region of the spectrum, L can be expressed as a brightness temperature *TB*, the temperature of a perfect black-body radiating the same amount of energy in the same wavelength range as measured by the radiometer. High count values on B3 data tapes correspond to low radiance or brightness temperature. L^* and *TB* are more convenient quantities because they are more directly comparable when measured by radiometers with slightly different spectral responses. The type of information available to convert the count values to radiances (or their alternates) varies from pre-launch calibration to active on-board calibration; Rossow *et al.* (1987) describes the best available information for each radiometer used by ISCCP as the nominal calibration of the radiometers.

Pre-launch calibration of the AVHRR solar channels (Channels 1 and 2) was performed with a standard calibration lamp viewed through an aperture in an integrating sphere; the calibration lamp is a standard traceable to NBS standards (Lauritson *et al.* 1979). The spectral output for the source lamp is known, allowing for correction of the calibration to the solar spectrum. We consider only Channel 1 here.

The pre-launch calibration establishes a relation between count values (representing instrument output voltage) and percent scaled radiance. Scaled radiance is the ratio of the radiance measured by the instrument and the effective solar 'constant' of the instrument. Radiances can be expressed as 'in-band' radiances representing the integral of the spectral radiance over the instrument response function and depending on the instrument response function, or as 'radiance per unit wave length' representing the 'in-band radiance' divided by the instrument bandwidth (Price 1987). Scaled radiance values do not depend on how the finite bandwidth of the instrument is treated (Rossow *et al.* 1987).

$$L_1^* = G_1(CT_8) + Y_1 \quad (1)$$

where CT_8 = 0 - 255.

For NOAA-7 AVHRR, the gain is G_1 = 0.4272 and the intercept is Y_1 = -3.440. For NOAA-8, G_1 = 0.4242 and Y_1 = 4.162. For NOAA-9, G_1 = 0.4254 and Y_1 = -3.846. Uncertainties are estimated to be about 5 - 10 percent

To obtain radiances the effective solar spectral irradiance for each channel is calculated by integrating over the product of the spectral response functions (see Rossow *et al.* 1987, §§7.1 and 7.2) and the solar irradiance table of Neckel and Labs (1984). (The original NOAA calibration uses a different solar irradiance table; small adjustments in the calibration coefficients have been made to correct for the change in tables (Rossow *et al.*, 1987).) Thus

$$L_1 = (E_{o1}/\pi)L_1^*/100) \text{ Wm}^{-2} \text{ sr}^{-1} \quad (2)$$

where E_{o1}/π = 56.66 Wm^{-2} sr^{-1} for NOAA-7, E_{o1}/π = 56.70 Wm^{-2} sr^{-1} for NOAA-8, and E_{o1}/π = 60.91 Wm^{-2} sr^{-1} for NOAA-9.

1.2.3. *ISCCP calibration monitoring*

The NOAA polar orbiter Advanced Very High Resolution Radiometer (AVHRR) data from Channels 1 and 4 play a crucial role in the project by serving as the radiometric calibration standard for all of the satellites. Although a thorough pre-launch calibration of all AVHRR channels is performed (see Kidwell 1988, Rossow *et al.* 1987), only the infrared channels are monitored after launch using an on-board calibration target. We show evidence for the stability of the Channel 4 calibration in Appendix A. At the beginning of the project, the absolute calibration of Channel 1 for the NOAA-7 AVHRR was not known.

Lacking a comprehensive field measurement program to establish an absolute calibration, the pre-launch calibration of Channel 1 was checked by comparing the surface reflectances obtained for a variety of surface types to available values reported in the literature (Matthews 1983, Matthews and Rossow 1987). In addition to uncertainties arising from surface and atmospheric effects that are not accounted for in the analysis, there is a degree of uncertainty in the reported literature values (Matthews and Rossow 1987). Often description of the measurements is incomplete, regarding the type of instrument used, its calibration, spectral response, relevant characteristics of the surface measured, viewing and illumination geometry, and (where needed) the corrections for atmospheric effects, such as broken cloudiness or aerosols. These factors are responsible for a large range of reflectance values reported in the literature for specific surface types. Despite these factors, there was sufficient agreement between visible reflectances obtained from NOAA-7 AVHRR with the published literature values to adopt the performance of the AVHRR Channel 1 on NOAA-7 in July 1983 as the standard reference for all visible radiance measurements in the entire ISCCP data set (Rossow *et al.* 1987). This calibration was later revised when better information was obtained (see §6.4).

To be able to use the Stage B3 radiances to determine a climatology of cloud properties, the radiances must be calibrated and the calibration maintained as a constant over the whole data set. In addition to the normalization of the geostationary satellite radiometers, this requires monitoring of the calibrations of the AVHRR over long periods. Since the polar orbiters are replaced periodically, the calibration standard must

also be transferred from one satellite in the series to the next. Both of these tasks are the subject of this paper.

1.3. *Outline of paper*

The methodology used to monitor the Channel 1 calibrations of a series of AVHRRs over long time periods and to normalize these radiometers to the reference standard is described. Results and corrections to calibration are given for the AVHRRs on NOAA-7, NOAA-8, and NOAA-9, covering a period from July 1983 through November 1988. Similar results are reported for Channel 4 calibrations in the Appendix.

Section 2 describes the targets, the radiative analysis applied to remove mean atmospheric effects on the radiances, the cloud algorithm used to divide the data into nominal categories of clear and cloudy, and the statistical tests and comparisons performed to detect any changes in AVHRR calibration. Section 3 illustrates the application of this technique to monitoring the calibration of NOAA-7 over a 19 month period. We also show evidence for the assumed stability of the global distribution of reflectance values. In Section 4, we adapt the procedure to normalize succeeding AVHRRs to NOAA-7; corrections for differences in mean solar zenith angle and calibration are examined for NOAA-8 and NOAA-9. In Section 5, the monitoring results for NOAA-8 and NOAA-9 are presented. We also present the complete time history of Channel 1 calibrations covering July 1983 through November 1988. In Section 6 we assess the uncertainties of this procedure, compare our results to independent studies, and discuss the use of intensive field measurements to provide an absolute calibration of all the AVHRRs.

2. Methodology

2.1. *Processing*

The data processing flow for both the monitor and normalization procedures is depicted in Figure 1. The normalization section of the flow chart (dashed lines) is discussed in §4. All of the B3 data are processed, representing approximately 20 million daytime image pixels per month per satellite. NOAA-7 data were acquired from July 1983 through early February 1985, NOAA-8 data from October 1983 through May 1984, and NOAA-9 data from January 1985 through early November 1988.

In the AVHRR monitor procedure, a spatial variability index is calculated first to classify the data as CLEAR or CLOUD. This classification is used to sort the data into three one-dimensional radiance histograms (TOTAL, CLEAR, CLOUD) for different surface types. Next, surface reflectances are retrieved from the radiances, and finally, a set of reflectance filters are applied to produce global surface reflectance maps. This approach provides two different samples of the data to cross-check any variation measured.

2.1.1. *Spatial variability index*

Cloud detection is accomplished by means of a spatial homogeneity test to produce radiance histograms for each target and by means of reflectance filters to produce the global reflectance maps. The reflectance filters were developed from the target reflectance distributions for July 1983 and 1984 and January 1984.

A spatial variability index is derived for each pixel by computing the absolute value of the difference between the reflectance of the pixel and the mean reflectance

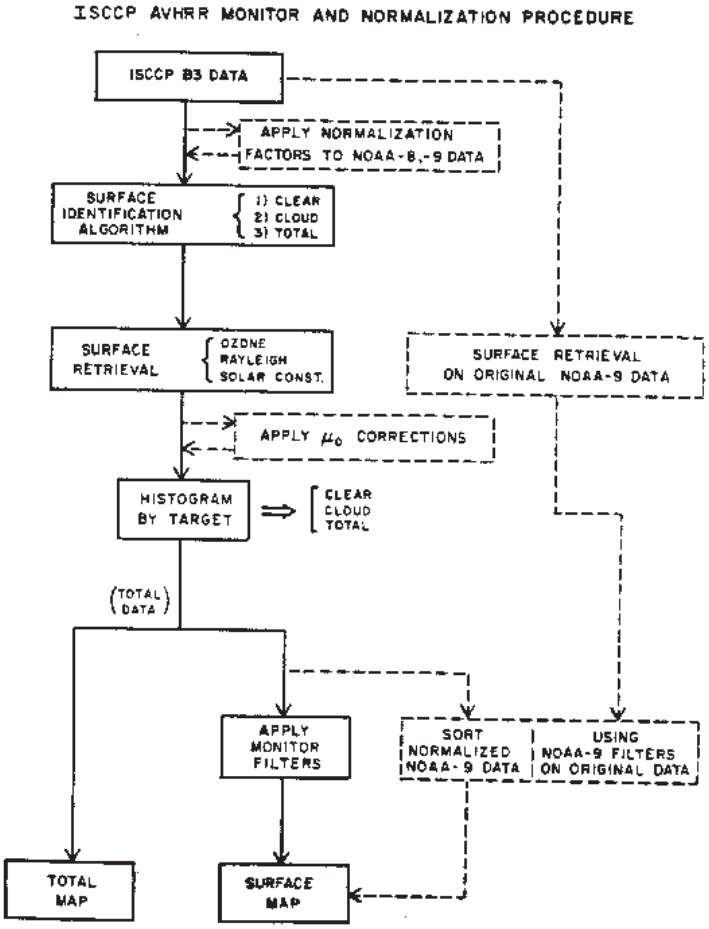

Figure 1. Flow chart of data processing for the AVHRR calibration monitoring (solid lines) and inter-satellite normalization (solid plus dashed lines).

for a 3 × 3 matrix centred on each pixel. If this difference is larger than a specified threshold value (0.015 for both land and water) the center pixel is classified as cloudy. Each pixel in the matrix is compared to its respective 3 × 3 matrix and the number of pixels whose reflectance difference is less than the threshold is determined. A high number (6-9) is classified as CLEAR (high homogeneity), while a low number (0-5) is classified as cloudy (high variability). Because the Earth's surface tends to have a smaller spatial variance than clouds (e.g., Coakley and Bretherton 1982, Desbois *et al.* 1982, Gutman *et al.* 1987, Sèze and Rossow 1990), this procedure generally gives a good indication of the presence of clouds in a scene. However, some cloud types, generally in the tropics, are relatively homogeneous (stratus) or optically thin (cirrus) and can be miss classified as clear scenes, while certain spatially variable surfaces (e.g., portions of the Sahara) can be missclassified as cloud. The statistical effect of a small amount of cloud contamination is negligible as shown

2.1.2. *Surface reflectance retrieval*

All data are then corrected for seasonal variation in solar irradiance, corrected for ozone absorption, and for Rayleigh scattering as a function of illumination and viewing geometry. This step produces a "surface" reflectance (whether clear or cloudy) and reduces variability by removing some of the angular, seasonal, and latitudinal dependencies of visible radiances at the top of the atmosphere. The radiative model used is the same as described in Rossow *et al.* (1989 b). The optical constants in the radiative models for visible radiance are adjusted to account for the spectral response of the NOAA-7 AVHRR Channel 1 and to simulate the observed spectral radiance as a function of viewing geometry. All optical properties are assumed to be homogeneous in a single AVHRR field of view, representing an area 4 × 1 km at nadir.

The only significant gaseous absorption within the bandpass of the AVHRR (Channel 1) visible channel is that by ozone (Lacis and Hansen 1974). The primary radiative process at this wavelength is scattering of solar radiation by gas and cloud. The clear atmosphere model has an ozone absorbing layer and a Rayleigh scattering layer. Ozone absorption is calculated using absorption coefficients taken from Inn and Tanaka (1953), the parameterization of Lacis and Hansen (1974), which corrects for the change in the spectrum of Rayleigh scattered sunlight with changing scattering geometry, and ozone column abundances as a function of latitude and month from the NIMBUS-4 SBUV climatology (Hilsenrath and Schlesinger 1981). The magnitude of the ozone correction for clear scenes is estimated to be 1-2 per cent for dark surfaces at low and middle latitudes and up to 5-10 per cent for snow and ice surface at very high latitudes (Matthews and Rossow 1987). Atmospheric Rayleigh scattering occurs in a layer with an optical depth proportional to surface pressure, assumed to be 1000 mb at all locations; for a clear column, the Rayleigh optical depth is 0.061.

A 'surface' reflectance is retrieved for all radiance measurements by comparing them to a table calculated from the visible radiance model with no clouds (cf., Rossow *et al.* 1989 b). This procedure neglects the anisotropy of cloud, land, and water surfaces; however, collection of observations over an entire month at varying geometries provides a stable statistical measure of these reflectances as shown in §3. Application of this retrieval procedure to cloudy scenes in not meant to be accurate and is done for computing convenience; however, the aggregate monthly statistics for clouds scenes also appear stable. Subsequent analysis focuses on the clear observations; however, the distribution of the cloudy radiances are also monitored for consistency with conclusions obtained from the clear reflectance values.

Although atmospheric effects on the satellite-measured radiances are rather small at 0.6 μm, they can introduce systematic errors that interfere with detection of small surface changes. Therefore, the accuracy of surface reflectances is dependent on the accuracy of the radiative transfer model used to remove the atmospheric effects. The accuracy of the clear scene, narrowband radiances simulated by the models for this study depends on the magnitude of three types of uncertainties (see Rossow *et al.* 1989 b for detailed discussions). First, model approximations to decrease computational load introduce errors which we estimate to be less than 1 per cent. Second, uncertainties in measurements of atmospheric properties used in the model, specifically estimates of uncertainty arising from ozone absorption computations, are less than 2 per cent. Finally, the third type of uncertainty is due to neglected effects of atmosphere or surface. The primary example for this study is the neglect of aerosols and any residual cloud contamination. Overall, this is estimated to be less than 5 per cent. A histogram for a typical target is shown in Figure 2. Because of the procedure

we adopt to filter clouds, the bright residual tails are not a problem. Our method is dependent on accurate isolation of modal reflectances and this is accomplished by our simple cloud detection scheme.

2.1.3. *Target histograms*

Reflectance frequency histograms are collected for nine surface/vegetation classes and 28 specific geographic targets. The data base used to sort each pixel by vegetation type is a global classification (with 1° resolution) compiled by Matthews (1983, 1984) and is based on the UNESCO hierarchical classification. For this research 32 major vegetation types (Matthews 1983) have been aggregated into nine vegetation

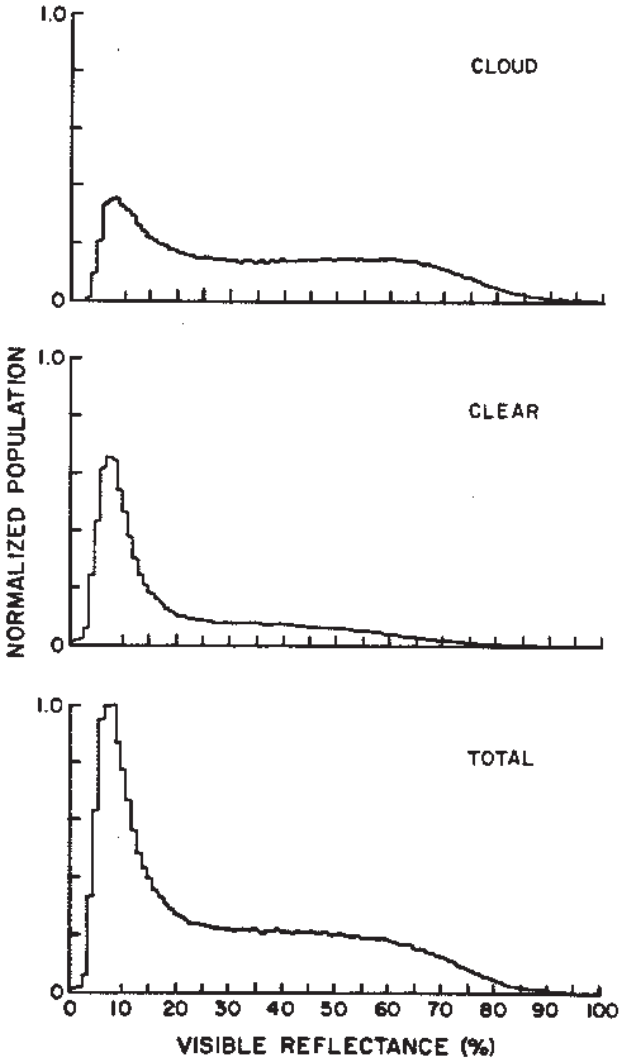

Figure 2. Sample histograms of a selected vegetation target (Deciduous forest, U.S.S.R. — July 1983) for the TOTAL category (all data) and CLEAR and CLOUD categories as determined by spatial variability test discussed in text.

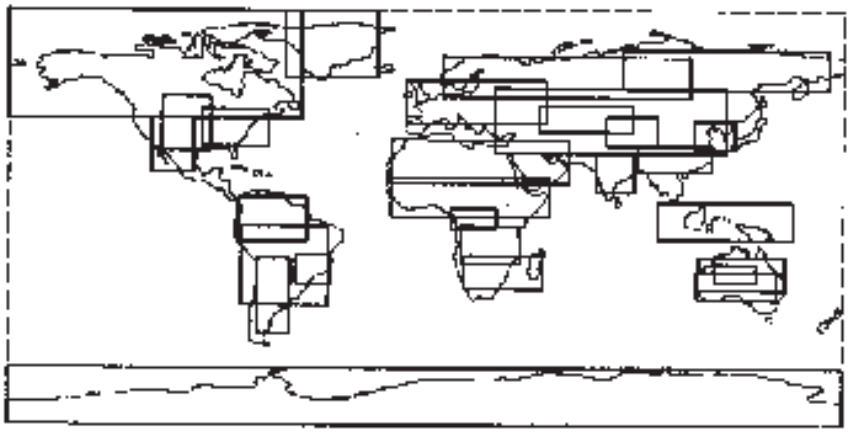

Figure 3. Map depicting the latitude/longitude windows used to define the 28 regional targets used in the analysis.

(ie., surface) "classes" based on characteristics of canopy structure and surface morphology. Previous work has demonstrated the importance of canopy structure in remote sensing of vegetated surfaces (Kimes 1983, Kimes and Kirchner 1983, Brest and Goward 1987, Brest 1987). Thus, the basic distinction is between tree canopy and low-canopy height vegetation: grassland, shrubland, and tundra. Three tree-canopy vegetation classes are defined: deciduous, evergreen, and rain forest. Lastly, the distinct morphological surface classes of desert, snow/ice, and water are also defined.

These nine vegetation classes are further divided into geographic "targets", representing distinct regional and hemispheric occurrences of each class, to avoid problems of contamination of the class due to seasonal climate changes in cloud cover or snow cover, to derive a better (ie., more specific) set of reflectance filters for the cloud detection step that avoids variations of a single vegetation type from region to region, and to separate seasonal illumination effects by monitoring the same surface types in the northern and southern hemisphere. Additionally, certain higher latitude areas are not available year round.

A total of 28 surface targets are chosen. Each target consists of the occurrence of the appropriate land cover type within the latitude/longitude windows shown in Figure 3. The number of targets per class is variable ranging up to seven for one class. These targets are well distributed geographically, and comprise the bulk of the earth's land areas. The complete list of vegetation classes and targets (including the latitude/longitude boundaries used to define them) are given in table 1.

A third set of 'targets' is also defined to encompass larger areas (ie., continents, hemispheres) with no breakdown by surface type. This target set includes the entire globe, all land surfaces, hemispheres, hemispheres subdivided according to land and water, and individual continents. Complete sets of histograms are also produced and examined for these targets, although they are not used directly in the calibration comparisons.

Three histograms are produced for each target: TOTAL, CLEAR, and CLOUD. For each histogram the following are determined: histogram population, mode reflectance value and frequency, the 10th, 25th, 50th, 75th, and 90th percentile reflectance values, the "half-mode" points (reflectance values at which the frequency first

falls below half of the mode frequency), the population and mean within the range defined by the "half-mode" points and in the range defined by twice the distance of the "half-mode" points from the mode, the proportion of pixels within both the "half-mode" and "twice half-mode" ranges, and the proportions of pixels categorized as CLEAR and CLOUD. Histograms are also produced for the three angles involved: μ_0 (cosine of the solar zenith angle), μ (cosine of the satellite zenith angle), and ϕ (the relative azimuth angle). All of these histograms are produced for each month of data for each satellite.

The variability of the CLEAR reflectance histograms with time is examined for larger regions and for different surface types. Since the spatial variance test eliminates most of the clouds, most of these histograms exhibit relatively narrow distributions of reflectances, associated with actual surface properties (Matthews and Rossow 1987, Rossow *et al.* 1989 a, Sèze and Rossow 1990). Some histograms exhibit broader distributions, but the shapes are constant with time (e.g., similar mode, half-mode, and percentile values for July 1983 and July 1984).

2.1.4. *Reflectance filters*

The temporal stability of the CLEAR reflectance histograms is used to define reflectance limits for each surface type and/or vegetation class, and each geographic target or region. The distances from the mode reflectances to the halfmode frequency values are doubled to define the filter limits. The procedure is conducted independently below and above the mode. These filters are then applied to the original data (not just the CLEAR data) to remove clouds to produce global maps of surface reflectance. Note that regardless of the histogram classification, a pixel is included in the surface map if it passes the reflectance filtering step. With this procedure measurements of a highly variable surface can be included if its overall reflectance is within

Table 1. Vegetation/surface classes and targets used in AVHRR monitor.[†]

Classes	Targets
Water	
Rain forest	Amazon (10S-10N,80W-50W), Africa (5S-5N,10E-30E), Asia (9S-8N,97E-156E)
Deciduous	Southeast United States (31N-47N, 96W-66W), South America (29S-15S, 56W-40W), Europe (41N-60N, 9W-51E), Africa (20S-3S, 14E-40E), India (11N-29N, 71E-88E), China (30N-43N, 12E-131E), U.S.S.R. (55N-73N, 82E-172E)
Evergreen	China (20N-32N, 89E-122E), North America (43N-90N, 179W-52W), Eurasia (52N- 70N, 6E-112E)
Grassland	United States (29N-53N, 113W-91W), South America (38S-3S, 79W-41W), Central Africa (0N-18N, 16W-52E), South Africa (31S-16S, 15E-49E), Eurasia (28N-57N, 28E-128E), Australia (31S-16S, 115-153E)
Shrubland	North America (19N-43N, 118W-98W), South America (50S-17S, 18W-43W), Eurasia (37N-49N, 47E-87E), Australia (35S-22S, 14E-150E)
Desert	Sahara (15N-35N, 16W-60E), Gobi (31N-45N, 75E-98E), Australia (28S-19S, 122E-141E)
Ice	Antarctica (90S-65S, 180W-180E), Greenland (60N-90N, 60W-20W)

[†] Within the target boundaries defined by the indicated latitude/longitudes, only those locations classified as the named vegetation/surface class are included.

the filter limits. Also, spatially homogeneous cloud cover in some locations can be eliminated if its reflectance exceeds the range of the filters defined by the specific surface type. This procedure yields a more reasonable sample of clear-sky surface reflectances than a minimum brightness/maximum temperature approach which is too vulnerable to errors produced by spurious extreme values (Rossow *et al.* 1989 b, Sèze and Rossow 1990). The NOAA-7 filters for all targets are based on data from July 1983, January 1984, and July 1984 data to cover the range of natural, seasonal variations (excluding snow cover), which are generally small at 0.6μm (Brest 1987, Matthews and Rossow 1987, Rossow *et al.* 1989 a). The target histograms are designed to detect relatively large changes in calibration that would be evidenced by changes in the mode reflectances and target histogram populations. A 'small' change (or drift) in calibration is detected by shifting populations and modes within the reflectance filter ranges for each target and changes in mean reflectances of the global surface reflectance maps. These kinds of changes are the most likely to occur. We use double the "half-mode" range to obtain sufficiently wide filters to allow for some shifting of the data distribution. Selection of too narrow a range of filters could cause false variations associated with changes in vegetation phenology, residual cloud contamination, instrument noise, neglected atmospheric effects (eg., aerosols), and neglected surface effects (eg., anisotropy). Except for phenology, the magnitude of most of these factors has already been discussed (Matthews and Rossow 1987, Rossow *et al.* 1989a, Holben *et al.* 1986). Seasonal variations in vegetation reflectance in the visible channel are small, on the order of several percent (Brest 1987, Matthews and Rossow 1987), but allowance must be made for them. On the other hand, selecting too broad a filter set creates difficulties in monitoring from inclusion of seasonal cloud cover or snow. Further safeguards are provided by analyzing both histogram and map comparisons for the TOTAL data, ie., we also monitor the entire unfiltered data set. Any major change in calibration must be consistent across all of the results.

2.1.5. *Maps*

The reflectance filters are used to sort data into global maps with a latitude/longitude grid of ½ degree resolution. Four maps are created: monthly mean SURFACE reflectance, two bi-weekly SURFACE reflectance maps representing the first and second half of the month, and a mean TOTAL reflectance map which represents an average of all the data available for the month. The monthly mean SURFACE maps are used in a variety of comparisons: month to previous month; month to July 1983; and month to same month of previous year(s). The bi-weekly maps are routinely compared to each other to detect shorter term variations. To date no calibration changes occurring on that time scale have occurred. The TOTAL reflectance maps, representing the entire data set with no classification, are produced to detect and assess any systematic biases which might be introduced by our processing.

In addition to the output products listed, a number of other variables are tracked to check the procedure. These include the total number of scan lines of data, the number of pixels examined, the number pixels flagged as nighttime, the number of pixels classified by the filters as surface (or clear) for the reflectance maps, the number of surface retrieval reflectance values which are less than zero and greater than 100 per cent. These quantities, together with the individual target pixel populations,

are examined to ensure that results are not governed by changes in data quality or distribution.

This method is used to monitor the calibration of NOAA-7, NOAA-8 and NOAA-9 and, in a slightly modified form (see §4), to normalize NOAA-8 and NOAA-9 to NOAA-7.

2.2. *Sensitivity analysis*

To assess our ability to detect and subsequently correct for changes in calibration we ran a series of sensitivity tests. Using a week of data from July 1984 we analyzed a total of sixty three cases of synthetic calibration changes. Both gain (multiplicative) and offset (additive) calibration changes were applied to the data, separately and in combination. The offset changes applied to the data were to add and subtract 1, 3, 5 counts (representing 0.4, 1.2, and 2.0 per cent reflectance, respectively). The gain changes were 0.95, 0.97, 0.98, 0.99, 1.00, 1.01, 1.02, 1.03, and 1.05. The changed datasets were then compared to the original using a linear regression analysis (see discussion in §3.1). For each case the slope and intercept of the best linear fit, means and standard deviations, root mean square deviations, and dataset populations are calculated together with the target reflectance histograms. Results are described for only a few of the key variables to illustrate important points.

A key feature of these results is that the magnitude of the changes in the reflectances is not the same for decreases in instrument sensitivity as for increases. This non-linear response occurs because the perturbations are applied to the radiances (as would occur with an instrument calibration change) but these values are converted to reflectances by dividing by μ_0. Secondly, the magnitude of darkening of already very dark targets (eg. water, rain forest) is constrained by the response of the instrument (negative radiances are not possible); whereas the brightening magnitude is not usually limited (except for a very few bright clouds). Gain decreases do not produce negative counts, while large negative offsets can; thus, the effect of the two types of calibration change is very different. Because the population of water measurements is so large and is limited by this effect, we also compare global maps by excluding all water points for cases where darkening has occurred. The non-linearity of the response of the reflectance statistics to a calibration change also means that we cannot use the slope/intercept values from the map comparisons directly as calibration correction factors.

The results of the sensitivity tests suggest that our method is sensitive enough to detect calibration changes as small as 2 per cent. Within this range there can be several values of the gain/offset corrections that produce equally acceptable results. The results also suggest several other conclusions:

- *(a)* the high accuracy of the results is produced by the statistics of a large data volume;
- *(b)* the effects of changes in gain and offset are distinctive;
- *(c)* the large range in target brightnesses allows for a more detailed examination of the calibration changes and provides cross-checks not available using a single target.

3. Monitoring NOAA-7

This section illustrates the application of the monitoring procedure and the use of the various statistics produced for checking the calibration with the results from 19 months of NOAA-7 data, covering the period from July 1983 through January 1985.

3.1. *Comparison of monthly data sets*

Three separate series of comparisons of the monthly global SURFACE reflectance maps were performed in the analysis of the NOAA-7 data: month to previous month, month to July 1983, and month to previous year (ie., the same month one year earlier). Each comparison was conducted by producing a scatter plot of the reflectance values from corresponding points in the two maps, calculating the correlation, mean and standard deviations, and fitting a straight line to the points by a least-squares criterion.

Each grid cell of the SURFACE map is an average of a much larger number of pixels. Of the approximately 20 million daytime pixels for a month of data, approximately 40 per cent or 8 million are typically classified as clear sky and put into the SURFACE regression map. (This yields a global mean cloud amount of approximately 60 per cent which agrees with the cloud cover amount based on the ISCCP operational cloud algorithm.) The number of grid cells in the SURFACE map containing data varies seasonally between 170,000 and 210,000, so that the number of data values averaged into each cell ranges from 40 to 50. The actual number of data points in each cell varies widely over the globe, depending on local cloud cover.

The results from the month-to-previous-month regressions show very high correlation coefficients, all values ≥ 0.98, reinforcing the supposition that the surface reflectances are very stable. Also the small root mean square error (all values ≤ 2.5 per cent) associated with these regressions indicates only a small amount of local variability. Month-to-previous-month variations are small, with all values being within 2 per cent of the perfect agreement line (ie., slope = 1.0, intercept = 0.0), while one third of the slopes are within 1 per cent of that value. That these values are indicative of systematic seasonal changes in surface conditions (phenology, snow contamination), solar zenith angle, and atmospheric components (aerosols and ozone), rather than variations in radiometer sensitivity, is indicated by the seasonal oscillation of the slope values themselves and by the comparison of July 1983 to July 1984 (see below) and all other months to previous years. Thus the small variations from month to month indicate no major, short-term changes in NOAA-7 radiometer performance during this time period. However, this particular comparison is not sensitive to a slow gradual drift of the radiometer calibration.

The second set of comparisons compares each month to July 1983. Again correlation coefficients are high, although they are lower for the winter months; no coefficient is below 0.90. The variation of the regression slopes are more indicative of the seasonal variation of surface reflectance with solar zenith angle: the slope decreases to 0.888 for December 1983, returns to 1.000 for July 1984, and decreases again to 0.851 for December 1984. This is consistent with increasing reflectance of most surfaces at higher solar zenith angles (Kriebel 1979, Kimes 1983, Eaton and Dirmhirn 1979) and to some snow cover contamination.

The third set of regressions performed is of each month to the same month in the previous year. The first comparison in this set, July 1983 to July 1984 (figure 4), is highly significant because the slope and *Y*-intercept of 1.000 (0.52) indicate little change in radiometer sensitivity over the first year of data collection. (We will use this convention throughout to indicate regression line slope (*Y*-intercept in per cent) values.) The *Y*-intercept value indicates that the July 1984 data may be slightly, ie., one-half percent, darker than the 1983 data. This is an important comparison because it is the first monthly comparison made under similar solar viewing geometries (except for drift in satellite orbit). The stability of the instrument over this time period

allows us to use this first year as a basis for comparison with future years of data, ie., to neglect solar zenith angle variations with season (see §6).

The remaining values from August through January all have slopes within 1.5 per cent of the 'no change' value. The last month of NOAA-7 data (January 1985) compares well to January 1984 data: 1.009 (0.27). The general indication is that the radiometer sensitivity has remained fairly stable over the last half year of data collection. An independent study over a longer data record suggests that there is a very slow (at most 1 per cent) decline in sensitivity of the NOAA-7 AVHRR (see §6.3); however, these results are within our 2 per cent uncertainty estimate.

3.2. *Visible reflectance histograms*

Histograms are also produced for each month of data for four parameters: visible reflectance, solar zenith angle, satellite zenith angle, and relative azimuth angle, although only the reflectance histograms are discussed.

Not only is the Earth's surface temporally stable, but even the TOTAL histograms for July 1983 and July 1984 (figure 5) indicate no change or a slight decrease in reflectance in July 1984. Approximately half of the targets which were histogrammed show no change in mode reflectance, while the remainder show a slight decrease in mode value, generally equal to 1 per cent. Some of the brighter targets such as the Sahara show a decrease in mode reflectance of 2 per cent. The large-area histograms show similar results. Categories such as earth, water, etc. show no change in modal value, while some of the land targets show a slight decrease. The January 1984-January 1985 comparison of visible radiance histograms also indicates the same relative

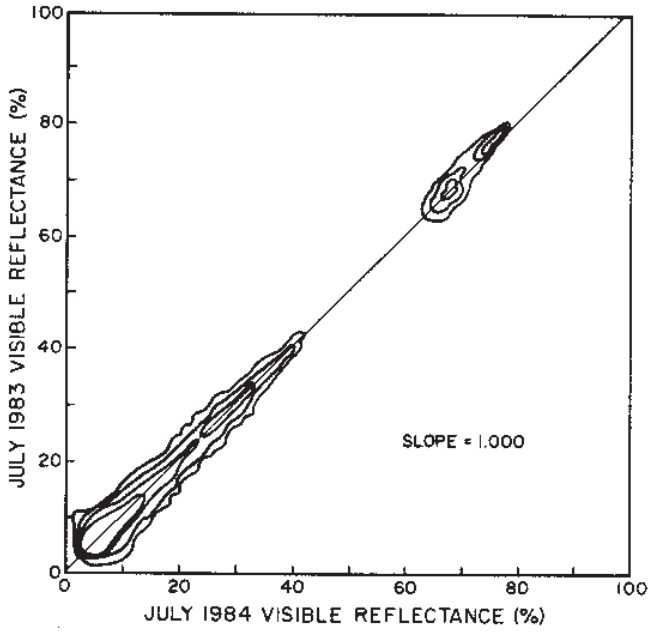

Figure 4. Regression of global SURFACE reflectance maps for July 1983 and July 1984 from NOAA-7 AVHRR Channel 1 data. Best fit least-squares linear regression is shown as solid line.

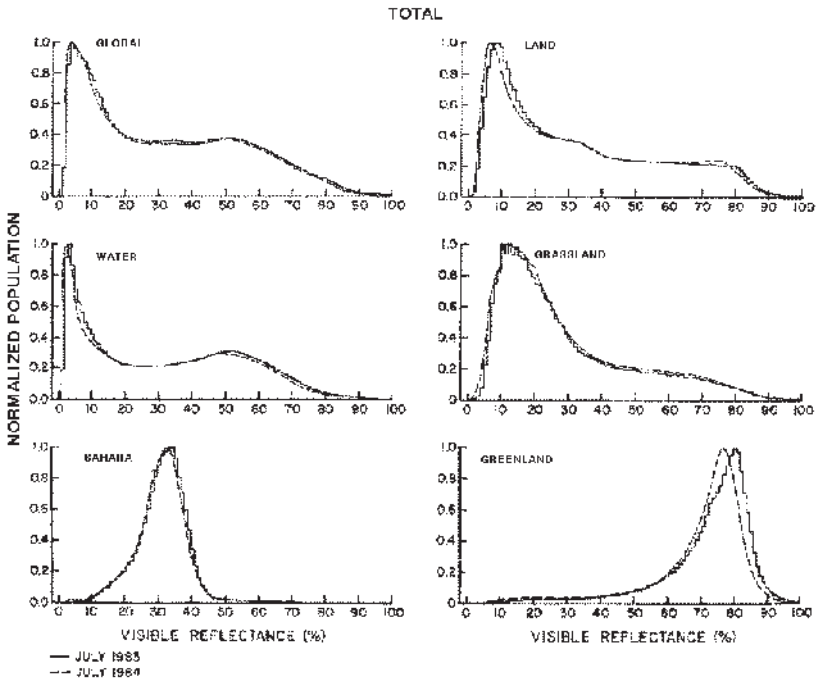

Figure 5. Comparison of histograms of visible reflectance for July 1983 (solid) and July 1984 (dashed) for TOTAL for selected targets.

stability for both the CLEAR and TOTAL cases. The temporal stability of the Earth's surface is the key to the monitoring of relative calibration: despite local variability a multitarget statistical procedure, such as described here, can properly take advantage of this global stability.

3.3. *Target reflectance*

Mean reflectances from the SURFACE map for the Earth, land, water, and selected targets from the time periods in question are presented in table 2. These tar-

Table 2. Comparison of July 1983-July 1984 and January 1984-January 1985 per cent reflectances for selected targets

	Surface mean visible reflectance									
Period	Global	Land	Water	RF	DEC	EVG	GRS	SAH	ANT	GRN
July 1983	9.5	15.2	6.7	5.6	8.9	8.9	13.8	30.4	0.0	74.3
July 1984	9.0	14.6	6.2	5.1	7.7	8.3	13.5	29.9	0.0	71.6
Jan 1984	16.9	39.8	5.9	5.7	13.5	13.2	16.2	30.7	78.1	76.7
Jan 1985	16.4	39.0	5.6	5.4	12.8	13.1	16.2	30.8	76.6	76.0

RF = rain forest, DEC = deciduous forest, EVG = evergreen, GRS = grassland, SAH = Sahara, ANT = Antarctica, GRN = Greenland

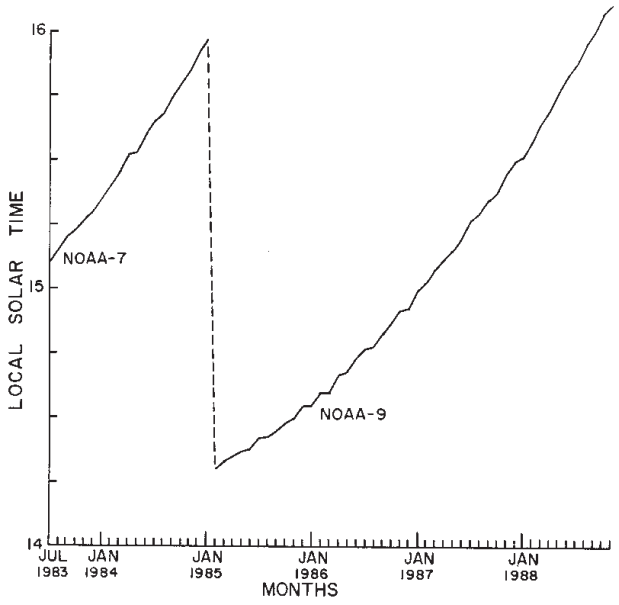

Figure 6. Time history of ascending equator crossing times for NOAA-7 and NOAA-9.

gets are selected as representative examples of a particular surface class and will be used throughout the paper to summarize the results. The selected targets are water, rain forest—Amazon, deciduous forest—U.S.S.R., evergreen forest—North America, grassland—Eurasia, desert—Sahara, and snow/ice—Greenland and Antarctica. The July-July comparisons show a slight darkening in 1984. Most of the targets show a decrease of about 0.5 per cent, with the exception of Greenland. The Jan.-Jan. comparisons vary from no difference to a slight darkening, again approximately 0.5 per cent, larger for the snow/ice targets. A second comparison was made using global mean reflectances, which also shows a darkening of 0.5 per cent.

3.4. *First 19 months of data analysis*

The radiative transfer model used in the monitor to obtain surface reflectances does not account for surface angular anisotropy. However, the averaging of several observations, which combines measurements from different viewing geometries, decreases but may not eliminate all angle dependance. Two effects due to μ_0 are noted in AVHRR data: the seasonal variation and a variation over a 9 - 10 day cycle due to the location of the target within the orbit swath (Gutman 1987). The systematic solar zenith angle dependance with season is not removed, as evidenced by the seasonal variation in the map reflectance and target statistics, while the latter effect is included in the averaging which is performed in the analysis. An additional systematic effect is the drift in orbit over the first year of data collection (see figure 6), which results in a general increase in solar zenith angle. The mode for the global distribution decreases from $\mu_0 = 0.79$ to 0.70. Given this change, one would predict a slight brightening of the data for July 1984 as compared to July 1983 based on higher reflectances

at lower μ_0 (Kriebel 1979, Kimes 1983, Eaton and Dirmhirn 1979). However, a slight darkening is evident in the results presented thus far. We feel that there may have been a slight degradation of radiometer sensitivity (of the order of 1.0 per cent) during this time period which has effectively countered the expected trend based on angular considerations. This effect is very small, and well within our estimated uncertainty (but see §6). Therefore, based on our examination of the combination of monthly regressions, histograms, and mean reflectance values, we conclude, that within the error limits, there was no significant drift in NOAA-7 AVHRR channel 1 sensitivity during the first 19 months of ISCCP data collection.

4. Satellite normalization

4.1. *NOAA-9*

4.1.1. *Initial comparison of calibrations*

NOAA-7 served as the ISCCP normalization standard through January 1985. In February it was replaced by NOAA-9. In order to maintain a uniform calibration over the life of the project, it is necessary to normalize NOAA-9 to NOAA-7. For this purpose three weeks of overlapping data were obtained, the last two weeks of January and the first week of February (Jan. 18 - Feb. 8, 1985).

The first step in assessing the difference between the calibrations of NOAA-7 and NOAA-9 AVHRR's was to process the three weeks of overlap data for both with the monitor software. Next the two global SURFACE reflectance maps were compared (figure 7). The resulting slope of 0.896 indicates a substantial calibration difference; a LAND ONLY comparison (slope of 0.902) also indicates a significant difference. This difference is also evident in all of the histograms as a shift in distributions of reflectance and in the mean reflectance for all targets (table 4). The differences are greater at the brighter end of the scale, which suggests that the calibration difference includes a difference in sensitivity (gain).

4.1.2. *Deriving solar zenith angle corrections*

At the time NOAA-9 was launched, NOAA-7 had drifted to a much later equator crossing time than the nominal 14.30 LST. At the beginning of the ISCCP data collection period in July 1983 NOAA-7 had an equator crossing time of approximately 15.05 LST. By January 1985 the crossing time was 16.00 LST, almost a full hour later. NOAA-9 had a 14.20 LST crossing time in January 1985 which also drifted

Table 3. Test cases of normalizations of NOAA-9 to NOAA-7. Shown are the best fit linear regression slope and *Y*-intercept obtained when surface reflectance maps from NOAA-9, with the indicated normalizations, are compared to those from NOAA-7.

Multiplicative					Multiplicative and additive				
	Global		Land only			Global		Land only	
Case	Slope	*Y*-intercept	Slope	*Y*-intercept	Case	Slope	*Y*-intercept	Slope	*Y*-intercept
nominal	0.843	-0.05	0.856	-1.05	nominal	0.843	-0.05	0.856	-1.05
0.885	0.990	1.20	0.989	1.21	0.850+2	0.967	0.06	0.983	-0.95
0.880	0.998	1.34	0.988	1.91	0.840+2	0.983	0.17	0.999	-0.84
0.875	1.003	1.32	0.993	1.88	0.835+2	0.989	0.16	1.005	-0.82
0.870	1.012	1.42	0.999	2.15	0.830+2	0.999	0.27	1.015	-0.74

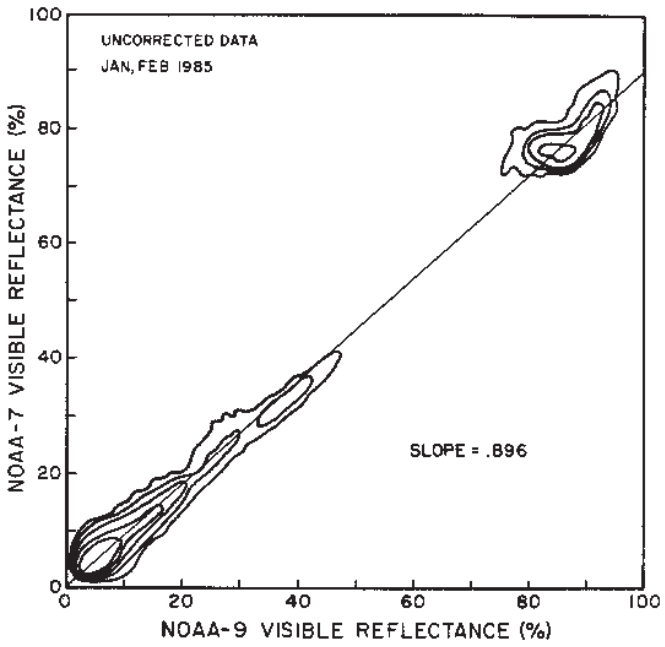

Figure 7. Regression of NOAA-7 and uncorrected NOAA-9 global SURFACE reflectance maps for the overlap period.

and reached approximately 16.07 LST by November 1988. The hour and forty minute difference in equatorial crossing times (figure 6) implies a difference in solar geometry between the two satellites during the three week overlap period.

The resulting difference in μ_0 (cosine of solar zenith angle) is illustrated in figure 8 which shows a comparison of the μ_0 histograms of NOAA-7 and NOAA-9 during

Table 4. Comparison of NOAA-7 and NOAA-9 mean SURFACE visible per cent reflectances.

			Normalized							
		Non normalized	Multiplicative only				Multiplicative and additive (+ 2 counts)			
	NOAA-7	NOAA-9	0.885	0.880	0.875	0.870	0.850	0.840	0.835	0.830
Global	19.0	22.6	18.1	18.0	17.9	17.7	19.6	19.2	19.1	18.8
Land	44.7	53.4	44.0	43.3	43.1	42.6	46.4	45.6	45.3	44.7
Water	4.0	4.6	2.8	2.7	2.7	2.7	4.0	3.8	3.8	3.6
Rain forest	8.0	14.2	11.6	11.5	11.4	11.3	12.0	11.7	11.6	11.5
Deciduous	51.3	57.0	40.5	38.6	38.5	37.6	51.9	50.4	50.3	48.8
Evergreen	45.9	55.1	43.7	43.0	42.8	42.2	48.2	47.1	46.8	46.1
Grassland	26.6	31.7	26.3	26.1	25.9	25.5	27.2	26.7	26.5	26.3
Sahara	30.8	37.2	31.8	31.6	31.4	31.1	31.7	31.2	31.0	30.7
Antarctica	75.7	90.8	77.5	76.9	76.5	75.8	78.2	77.0	76.4	75.8
Greenland	76.8	84.3	59.0	53.6	53.5	52.3	79.1	77.1	77.0	74.9

All data from January and February 1985. All data are μ_0 corrected.

the overlap period for the earth, land, water and a few selected targets. The histograms for the earth exhibit a difference between modal values of 0.34. The μ_0 differences for the selected targets range from 0.34 for lower latitude targets to nearly 0.0 for higher latitude targets.

Because of the significant difference in μ_0 between NOAA-7 and NOAA-9, we develop corrections for varying solar zenith angles by analyzing one year of NOAA-7 data (July 1983-84) for eight targets representing the major vegetation and surface types. Two dimensional histograms of surface visible reflectances (obtained by using the monitor filters to remove cloud effects) versus solar zenith angle are collected for each month of data and composited into an annual aggregate.

Most surfaces exhibit lower reflectance at higher μ_0, consistent with other studies (Kriebel 1979, Kimes 1983, Eaton and Dirmhirn 1979). The exceptions are the two snow/ice targets. However, the NOAA-7, NOAA-8, and NOAA-9 μ_0 values are nearly identical at high latitudes.

To derive μ_0 correction factors, the data sets are clipped at $\mu_0 \leq 0.15$ to avoid overemphasis of unreliable results at very low illumination levels and a least squares linear fit constructed. The slope correction factors for the eight surface types are: water 0.01; rain forest, 0.01; deciduous forest, -0.03; evergreen forest, -0.03; grassland, -0.03; desert, -0.04; Antarctica, 0.14 and Greenland, 0.17. These are in units of per cent per 0.01 μ_0. For example, for a target with a slope of -0.04, a decrease in μ_0 of 0.10 would result in an increase in brightness of 0.4 per cent. For the two surface classes for which no major site was available, shrubland and tundra, we used the grassland value because this has the most similar canopy structure, an important de-

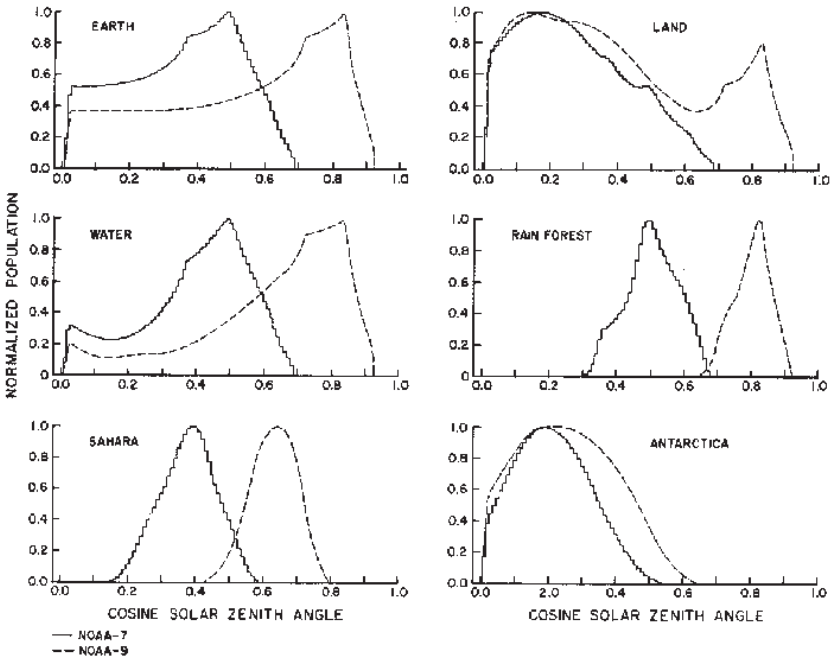

Figure 8. Comparison of histograms of cosine solar zenith angle for selected targets for NOAA-7 (solid) and NOAA-9 (dashed) data during the overlap period.

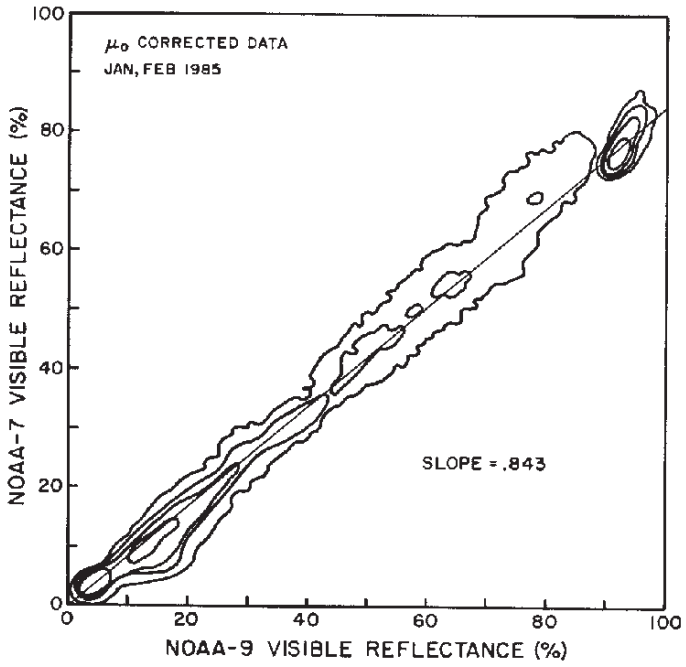

Figure 9. Regression of NOAA-7 and μ_0-corrected NOAA-9 global SURFACE reflectance maps for the overlap period.

terminant of the reflectance (Kimes and Sellers 1985, Kimes and Kirchner 1983, Brest 1987).

4.1.3. *Applying solar zenith angle corrections*

Reference μ_0 values are defined for each target by the average of the two modal values from NOAA-7 and NOAA-9. In a modified version of the monitor code, the reflectance of each pixel is corrected based on the difference between μ_0 and the reference value and the surface type slope correction factor. This correction is added (subtracted) from the original reflectance value to create the μ_0-corrected reflectance. The data are corrected to the reference μ_0 values for each target to minimize error introduced by the procedure. The effect of applying the correction to the NOAA-7 data is to increase μ_0 and decrease reflectances, for NOAA-9 it is to decrease μ_0 and increase reflectances. For example, the Sahara has μ_0 values of 0.39, 0.63 and 0.51 for NOAA-7, NOAA-9, and the reference value respectively, producing a darkening of the NOAA-7 mean reflectance by 0.5 per cent and a brightening of NOAA-9 by 0.5 per cent absolute. Most of the other surface categories would change by less than this. The regression comparison of SURFACE global reflectance maps is repeated using the μ_0-corrected data sets (figure 9). For the GLOBAL comparison the slope is 0.843 and the *Y*-intercept is -0.05. Comparing this slope to the previous value of 0.896 for non-μ_0-corrected data (figure 7), indicates that when solar zenith angle effects are properly accounted for, the actual difference in calibration is larger than the apparent difference. Similarly for the LAND ONLY case, the slope of 0.856 indicates a greater difference in the two maps than the previous slope of 0.902.

4.1.4. *Modified filter set*

The initial NOAA-9 to NOAA-7 comparison and the first attempts at normalization were performed using the NOAA-7 AVHRR monitor filter definitions to derive the global SURFACE reflectance maps for both satellites. The normalization procedure is as follows:

(i) the normalization factor (multiplicative and/or additive) is applied to the integer count value representing scaled radiance;
(ii) a new surface reflectance value is retrieved;
(iii) the NOAA-7 monitor reflectance filters are then applied to the resulting surface reflectances to eliminate clouds and produce the global SURFACE reflectance map.

A potential drawback to this procedure is that the population which falls within the filter range, and thus is included in the analysis, varies with the normalization factor. This may make the outcome unpredictable, because each comparison is to a different population of NOAA-9 data.

Although the results obtained using this procedure appeared acceptable, we confirm this by using a modified version of the analysis. In addition to differences in the radiometer response, there are two main factors which produce differences between the NOAA-7 and NOAA-9 data. The first is variation in clouds during the time span between satellite overpasses, while the second is difference in observed surface reflectance due to different solar geometry. The former is eliminated in our cloud detection step, while the latter effect is removed by applying the μ_0 correction to the data. (We ignore any slight variation in atmospheric properties during this short time span.) Thus, we have what are essentially simultaneous observations of identical targets. This allows us to define a separate set of reflectance filters for each satellite from the three week overlap data sets. This insures that the sample population for the comparisons is stable. The modified procedure requires us to perform the radiative transfer analysis twice, once with the original NOAA-9 radiance values (to be used with the NOAA-9 filters), and then again with the normalized values (which are compared to the NOAA-7 data). If a pixel's original NOAA-9 retrieved reflectance value passes the NOAA-9 filter test, then its normalized reflectance value is put into the global SURFACE map.

The new filters for NOAA-7 and NOAA-9 were derived in the same way as the monitor filters using modes and half-mode values. Many of the NOAA-7 filters are similar to the AVHRR monitor filters, but a few are significantly different because they include some snow cover or persistent cloud cover. The broader filters are advantageous for two reasons. First, because we have a limited sample (only three weeks) of data to work with, taken during Northern hemisphere winter when some of our targets are snow covered, the new procedure gives us a larger population to work with by defining the reflectance filters for the specific time period rather than for a whole year. Secondly, this approach gives us more data in the brighter range of reflectances, between the Sahara and snow/ice reflectances, which should be beneficial to our linear regression analysis. Both of these points are evident in a comparison of figure 9 to figure 7. The filters are defined separately for each satellite based on the modal populations. This gives two sets of independent, but analogous filters.

4.1.5. *Normalization*

The entire normalization procedure using the μ_0 correction and the new filters is shown schematically in figure 1 where the dashed lines represent the additional steps in the normalization version of the procedure. A variety of normalization factors, initially multiplicative and later multiplicative and additive, are tried. Selected examples are given in table 3 for both the GLOBAL and LAND ONLY comparisons. Because water reflectances are very dark, and because water comprises 70 per cent of the data set, it acts as a strong anchor point in the regression, allowing only the slope of the line to vary. Therefore, a second regression, LAND ONLY, is performed to assess this effect on the results. For reference the regression for the uncorrected comparison is also given. The choice of which factors provide the best normalization is made as a compromise between the best slope, best *Y*-intercept, and best mean reflectances for all of the targets.

For the four cases presented the slope varies from 0.990 to 1.012 for the GLOBAL case, and from 0.989 to 0.999 for the LAND ONLY case. All of these values are very close to a slope of 1.0 and all are preferable to the uncorrected case. On the basis of slope the best normalization factor is 0.880, if you consider only the GLOBAL case, and 0.870 for the LAND ONLY case. However, consideration of the *Y*-intercept values shows that all of them differ significantly from 0.0. They range from 1.20 up to 2.15, significantly enough to have an effect on darker reflectances. If we consider the mean target reflectances (table 4) a normalization factor of at least 0.885 would be better; however, the mean global reflectance still differs by almost 1.0 per cent. Also, the mean water reflectance for the normalized NOAA-9 data is significantly darker than NOAA-7, 2.8 per cent versus 4.0 per cent.

To remedy this we try a multiplicative and additive normalization. Regression results for four cases are given in table 3. The improvement is evident in the much smaller Y intercepts and the closer agreement of mean reflectance for both the GLOBAL and LAND ONLY cases. The resultant mean reflectances for individual targets, shown in table 4 for both the multiplicative and multiplicative and additive cases, are also much improved. Note also the close agreement with all other targets except for rain forest, which is still off by a few percent. Based on consideration of all factors (slopes, intercepts, mean reflectance values, for both GLOBAL and LAND ONLY cases), we selected the value of 0.835 + 0.2 per cent as the best compromise value (figure 10). The mean global reflectances differ by only 0.1 per cent.

Although much effort went into the selection of the normalization factors, the differences between reflectances given by the considered range of factors are actually fairly small. For instance, comparing the best multiplicative and the best multiplicative and additive corrections shows that the resultant differences in mean reflectance for water, desert, and Antarctica are 1.0, 0.8, and 1.1 per cent absolute, respectively. These differences provide estimates for the errors in these normalizations.

4.2. *NOAA-8 normalization*

NOAA-8 is a morning polar orbiter with nominal equator crossing times of 7.30 LST (local standard time) descending node (daytime coverage) and 19.30 LST ascending node (nighttime coverage). Eight months of NOAA-8 AVHRR data, from October 1983 through May 1984, were made available to the project to supplement coverage over the Indian Ocean sector. Global coverage is approximately 60 per cent complete. The AVHRR onboard NOAA-8 is a four-channel instrument, in contrast to

NOAA-7's five channel radiometer (Kidwell 1988), with the missing band in the thermal infrared region (for more detail see Rossow *et al.* 1987).

The initial NOAA-8 to NOAA-7 comparison of calibrations was performed using data from November 1983. For this GLOBAL comparison the slope and *Y*-intercept of the least squares linear regression are 1.009 (0.55), indicating an excellent correlation between the two data sets. The LAND ONLY regression also yields a very close relationship with a slope and *Y*-intercept of 1.003 (1.14). Thus the preliminary indication was that the calibrations of the two instruments were similar to within 1 per cent.

As a further check on this initial assessment, the TOTAL maps for each satellite were compared for the GLOBAL case. Although the natural variation in this data set is too large to allow its quantitative use in the normalization procedure, it does serve as a check on the normalization to see if we are biasing the results by our cloud elimination procedures. Variations in this data are primarily diurnal differences in cloud cover (afternoon versus morning) and anisotropic cloud reflectance. Although there is a much wider dispersion about the regression line for the TOTAL comparison (not shown), there is still a strong correlation of 0.90 between the two data sets. Further, the global mean reflectances differ by only 0.4 per cent, suggesting close agreement between the two instrument calibrations.

The differences between μ_0 modes are also much smaller than for NOAA-9, ranging from 0.0 to 0.12. Thus, the μ_0 corrections applied to the data were very small. The comparison of μ_0-corrected SURFACE maps yielded results which were virtually identical to the earlier results: slope and intercept of 1.009 (0.57) versus 1.009 (0.55) for GLOBAL; and 1.000 (1.34) versus 1.003 (1.14) for LAND ONLY.

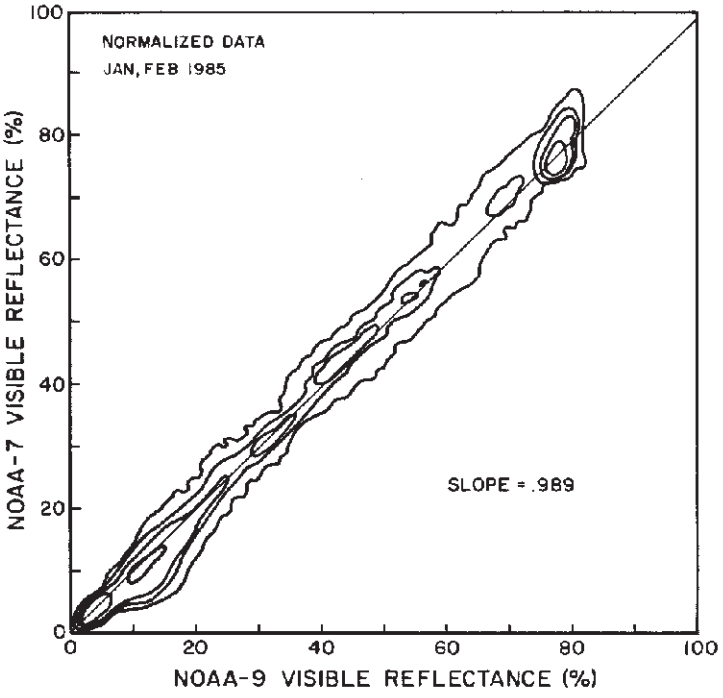

Figure 10. Regression of NOAA-7 and normalized NOAA-9 global SURFACE reflectance maps for the overlap period.

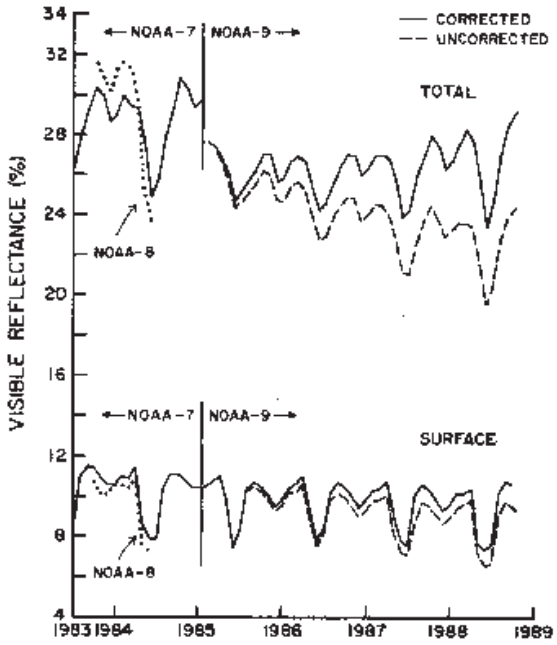

Figure 11. Time history of monthly mean global visible reflectance for both TOTAL and SURFACE derived from NOAA-7 (pre-Jan. 1985), NOAA-8 (dotted line), and NOAA-9 (post-Jan. 1985) data with correction (solid line) and without correction (dashed line) for NOAA-9 sensor degradation.

Since the slope and intercept in the comparison regression are not exactly 1.0 and 0.0, suggesting a small calibration difference, we introduce a normalization factor into the comparison to see if we can improve the relationship. Three cases were run, but results were not significantly different. Based on consideration of these results, we conclude that the differences in all of the cases studied and in the resultant data sets are well within the sensitivity and error limits of the method, and therefore the slight differences observed are probably not significant; and no significant improvements are achieved by attempting to normalize the NOAA-8 data to NOAA-7 data. Therefore, the calibration of NOAA-8 Channel 1 radiances is taken to be the same as that of NOAA-7 in November 1983 to within 2 per cent.

5. Satellite calibration monitoring

5.1. *NOAA-9 Monitor*

Having normalized the NOAA-9 data to that of NOAA-7, we then ran the AVHRR monitor on the normalized NOAA-9 data from February 1985 through November 1988 using the same set of monitor reflectance filters developed for NOAA-7. The application of these filters to the normalized NOAA-9 data yields populations which are similar when they are applied to NOAA-7 data.

In contrast to NOAA-7, which remained relatively stable (within the uncertainty), NOAA-9 immediately displays signs of sensor degradation. The global monthly mean reflectances for the period from July 1983 through November 1988 are displayed in figure 11 (labeled uncorrected) for both the SURFACE maps and the TOTAL maps. For the sake of completeness NOAA-8 data have also been included in

the diagram. The SURFACE maps display a seasonal variation associated with several factors. The primary driving force is the inclusion/exclusion of Antarctica which dominates the smaller effect of Greenland. Lesser factors are differences in solar zenith angle of the observations for land surface (low μ_0, brighter surface reflectance) in Northern hemisphere winter season and brightening of targets by the inclusion of some snow-covered surface within the reflectance filters. The TOTAL maps also display the same seasonality. The decreasing monthly mean reflectance for NOAA-9 is evident in both sets of maps, although the effect is more dramatic in the brighter TOTAL maps. The decline in reflectivity of the TOTAL maps confirms that the degradation of NOAA-9 AVHRR channel 1 is not the result of a bias introduced by our data processing. Although we have included the TOTAL map for display purposes, all of our results are based on the use of the SURFACE maps only.

Monthly mean reflectances for selected targets are shown in figure 12. Again both the seasonality (of some targets) and the degradation of the NOAA-9 sensor sen-

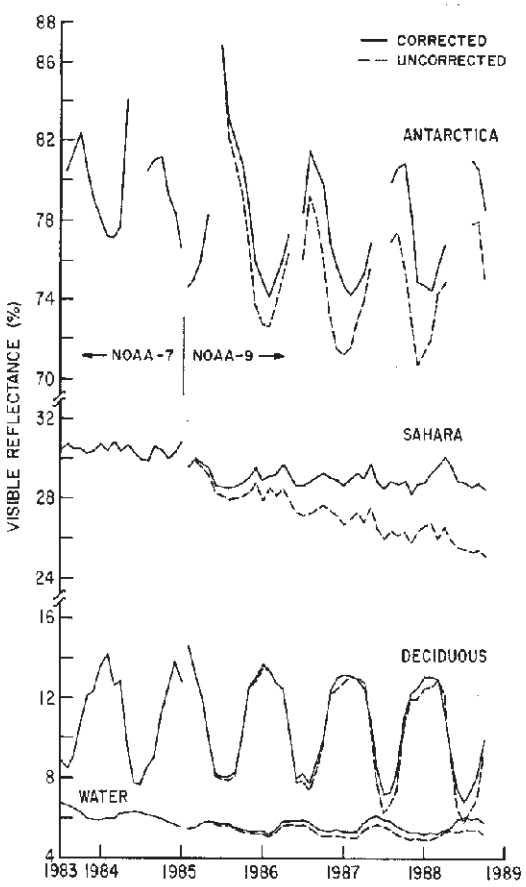

Figure 12. Time history of monthly mean SURFACE visible reflectance for four selected targets derived from NOAA-7 and NOAA-9 data for both corrected (solid) and uncorrected (dashed) cases.

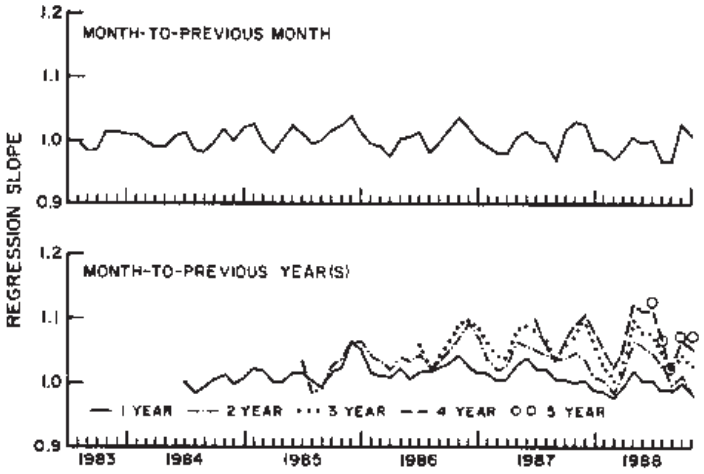

Figure 13. Time history of slopes from the linear regression analysis for comparisons of month to previous month (top), and month to previous year(s) (bottom).

sitivity (for all targets) are evident. Notice that the decline is larger for the brighter surfaces (compare Sahara to water), indicating that the effect represents a change in instrument gain. Although the snow/ice targets are highly variable, the decline in sensitivity is also apparent.

The change in instrument sensitivity is also evident in the monthly regressions performed in the AVHRR monitor. Figure 13 displays plots of the regression slopes for two sets of comparisons: month-to-previous-month, and month to previous year(s). In these comparisons, the current month is the *X*-variable while the previous month (or year) is the *Y*-variable. Therefore, a slope greater than 1.0 indicates that the current month is darker than the previous month (or year).

Examination of the month-to-previous-month regression slopes does not reveal any general trend, but the deviations from a slope of 1.0 appear greater for slopes larger than 1.0 than for those smaller. This can be illustrated by the cumulative application of these slopes to a given target reflectance; e.g., for a hypothetical target of 50 per cent reflectance, the succeeding month's reflectance is calculated by applying the inverse of the regression slope. A significant decline in reflectance is observed over time, reaching a low of 44 per cent at the end of the study period. This result reinforces the interpretation of the sensor calibration drift as a 'slow trend'.

Each month is also compared to the same month in the previous year or, if applicable, years. The increase in slope as the regressions are performed over longer time periods confirms a darkening of reflectances. Almost all slopes are greater than 1.0 with exceptions early in the one-year regression (from NOAA-7) and towards the end of the one-year regression.

5.2. Correcting for sensor degradation

We must correct for the observed sensor drift. Given the monotonic decrease in reflectance, we chose to fit a straight line to the data, using the monitor output from Feb. 1985 to Nov. 1988. Because of the seasonal variations of many targets it is necessary to use at least several complete seasonal cycles to derive a proper correction to the sensor degradation trend. We fit trend lines to the reflectance for a variety of tar-

gets, as well as the whole earth for both SURFACE and TOTAL cases. The slopes derived for each target were normalized by dividing by the target's mean reflectance.

Because of the global nature of the ISCCP project we chose the fit to the global map as the best compromise for all targets. Unlike the monitor, which is a relative comparison of data sets, we need the proper weighting of contributions from all surface types. Therefore, we calculate an equal area global map from the square latitude/longitude maps used in the monitor. The trend line for the sensor degradation was derived from global mean reflectance values obtained from monthly equal-area SURFACE reflectance maps. The slope of the fitted line was –0.03385 per cent and we normalize by dividing by the mean reflectance, 9.38 per cent, to yield –0.00361 per month. This value characterizes the sensor degradation we observe for Channel 1 of the NOAA-9 AVHRR for the period from Feb. 1985 to Nov. 1988. The accuracy of our trend line is confirmed by the close agreement between the resulting calibration and an aircraft absolute calibration obtained in November 1988 (see §6.6).

Using the trend line slope of –0.00361, we compute a monthly correction factor: 1/(1–0.00361) = 1.00362308. This monthly correction factor is applied successively to each month of NOAA-9 data starting in March 1985. The cumulative effect is such that by Nov. 1988 the correction factor for channel 1 has grown to 1.177.

The results of the application of these factors are shown in figure 11 as the corrected data. Both the need for and the suitability of the selected value of the monthly correction factor are clearly evidenced in this figure. The same results are shown for four targets in figure 12. Our hypothesis that the sensor degradation is primarily a change in gain and not an offset is supported by the similarity in reflectances for the dark targets, and the increasing difference for brighter targets.

5.3. *NOAA-8 monitor*

The NOAA-8 monitoring is performed in two ways: first, by examining the month-to-previous-month NOAA-8 comparisons (as was done for NOAA-7 and NOAA-9), and second, having already established the stability of the NOAA-7 sensor, by comparing NOAA-8 to NOAA-7 each month.

The month-to-previous-month comparisons for NOAA-8 indicate no trend in radiometer sensitivity. The comparisons between NOAA-8 and NOAA-7 indicate excellent agreement between the two satellite data sets over the whole time period. The mean SURFACE reflectance values agree very well; the average difference between global mean reflectances is only 0.6 per cent. Even the brighter categories are very similar in reflectance; the average monthly difference for the desert is 0.3 per cent.

5.4. *ISCCP B3 calibration tables*

As described in §1.2.1, three different calibration tables are available on each ISCCP Stage B3 data tape to convert the digital count values to radiances. The results of normalization are provided in the second set of calibrations ("normalized" calibrations), while corrections for long-term changes are provided in the third set ("absolute" calibrations). Figure 14 shows monthly mean reflectance for the Sahara as calculated using each of the ISCCP calibration tables. Note that for NOAA-7 (and also for NOAA-8, not shown) all three tables are identical, because no changes were needed. The nominal table represents the best available pre-launch calibration for the NOAA-9 AVHRR instrument. As discussed earlier, there is a significant difference in calibration between the two satellite instruments, and hence the jump in reflec-

tance. The second calibration table represents our normalization of NOAA-9 to NOAA-7, and hence the normalized reflectance is the nominal reflectance offset to the calibration of NOAA-7. Both of these calibrations contain the sensor degradation described earlier. The third calibration table contains the monthly correction factors applied to the normalized calibration table to produce the "absolute" calibration. The necessity for both the normalization and trend correction steps in producing valid climatological data sets is clearly evident.

6. Assessment of method and results

6.1. *Comments on method*

General requirements for a viable satellite calibration procedure are:

(a) a calibration standard which is well-defined and stable over time;
(b) a comparison to the calibration reference standard over most of the dynamicc range of the instrument;
(c) an examination of the linearity of the instrument response;
(d) a check for shifts in spectral response.

In addition, calibration checks must be performed frequently throughout the time period covered by the data obtained from the particular instrument. Specific features of our procedure address each of these criteria.

A fundamental assumption behind this analysis is that the global aggregate of regional variations of surface visible reflectance is not changing with time. Of course,

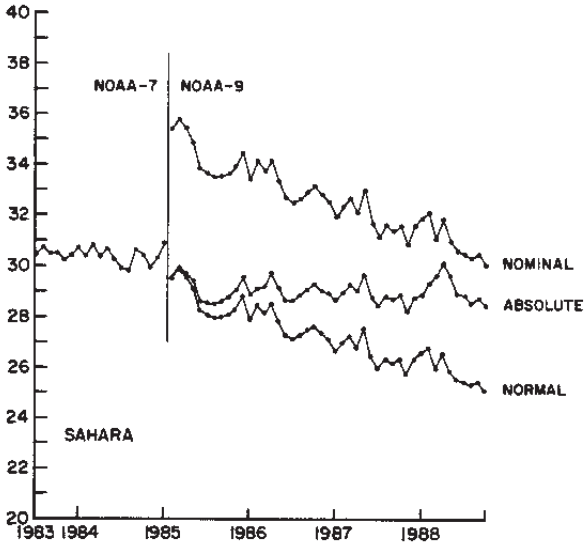

Figure 14. Time history of AVHRR Channel 1 (0.6 μm) calibration, shown as the reflectance of the Sahara desert measured by NOAA-7 and NOAA-9. The results are obtained as part of the ISCCP data processing, where NORMAL refers to the adjustment of te NOAA-7 and NOAA-9 calibrations during an overlapping period in January and February 1985, and ABSOLUTE refers to the correction for the sensor degradation.

on-going human modifications of the surface and climate are expected to cause some systematic changes in regional surface albedo; however, these changes are not expected to be very large, particularly at 0.6 μm, over periods of 5–10 years. Since we did not have a routine calibration program for the satellite radiometers at the start of ISCCP (such a program is beginning now, but is not yet fully established), the best available method to monitor calibration was the use of the earth's surface. The contrast in the results between NOAA-7 and NOAA-9 provides post facto support for this assumption by showing both how constant the global reflectance can be and how rapidly an instrument can change. We also did not have very accurate data on the reflectivity of various surfaces, so this analysis provides a calibration relative to a somewhat poorly defined standard. As discussed below, when a better absolute calibration is available, it can be easily applied to the entire data set.

A key feature of our method is that we do not rely on the constancy of the surface at any one location, but rather on the constancy of the global aggregate of targets. In effect, we use over 200000 individual targets (although all the water locations do not provide independent information) to check for calibration changes. We explicitly monitor not only the statistical variations (means and distributions) of a large number of surface types and various-sized geographical aggregations, but also the changes in each 50 km × 50 km map grid cell covering the whole globe.

This approach supplies both a massive statistical weight and a sensitivity to different kinds of instrument changes. The former ensures that only a change in the instrument would produce a systematic shift of all the measured quantities, whereas the latter enables the detection of changes in instrument linearity or spectral responses. Although we have not emphasized this aspect of the results and have calculated only linear shifts in calibration, we have not observed any changes in the character of the regressions that would suggest either linearity changes or spectral response changes. Figure 4 shows that the response of the instrument is very linear; moreover, the shifts in target mean reflectances do not indicate significant differences between water, vegetation, and deserts, which would appear with large changes in spectral response.

The wide variety of surface types also ensures that our measurements cover a large portion of the instrument's dynamic range. The clear sky radiances of some deserts areas are almost 50 per cent of the solar insolation. Our use of reflectances (radiance divided by cosine of solar zenith angle) makes the land ice sheets the "brightest" objects, even though their clear radiances are only about 20-30 per cent of the solar constant. This means that any discrepancies in radiance measurements will amplify discrepancies in reflectances for these locations. Figure 10 shows that our corrected calibrations produce very good results for these targets, too.

The resulting calibration measurements represent the best global compromise for all target types and reflectance ranges. By normalizing the entire ISCCP radiance data set to this standard and maintaining constancy over the whole time period, we ensure the best approximation to a uniform radiometric standard that is obtainable. Below we show additional evidence that this result is a good 'calibration'.

6.2. *Estimates of sensitivity/error*

We have conducted several tests and checked the internal consistency of our results to estimate sources of error and the detection sensitivity of the method. Figure 5 shows the difference of the TOTAL radiance distributions for one month, collected one year apart from NOAA-7. The distribution of point–to–point differences between

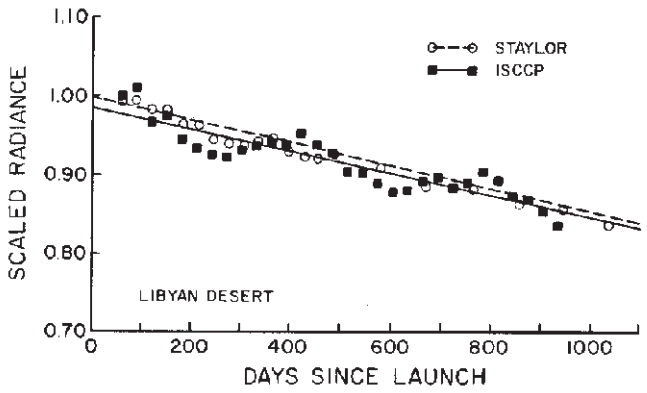

Figure 15. Comparison of the NOAA-9 sensor degradation as determined by the ISCCP method and by Staylor (1990) using the Libyan desert.

two global SURFACE reflectance maps, collected one year apart from NOAA-7, shows not only the radiometric stability of Earth and its surface as a target, but sets an upper limit of about 3 per cent (absolute) on the error in measuring a reference calibration.

The synthetic sensitivity study, discussed in §2.2, showed that the method was probably not able to detect a calibration shift smaller than 1 - 2 per cent (absolute) reliably, especially if the shift was due to a degradation of sensor sensitivity. Therefore, we chose to ignore any indications of calibration change smaller than 2 per cent in these results. However, a more careful examination of the NOAA-7 results and the longer-term monitoring results of Staylor (see below), shows that the NOAA-7 radiometer sensitivity actually decreased at a rate of about 0.5 - 1 per cent (absolute) per year. If we correct the NOAA-7 data for the effect of drifting equator crossing time on average solar zenith angles, we find a slight darkening of reflectances over a 19 month period of about 0.5 - 1.0 per cent, which is equivalent to a sensitivity decrease of about 0.3 - 0.6 per cent (absolute) per year. The fact that we apparently detected such a small decline suggests that our sensitivity and error estimate of 2 per cent is very conservative.

6.3. *Comparison to independent analyses*

Results from two independent analyses are available to assess the accuracy of our AVHRR Channel 1 monitoring procedure. First, Staylor (1990) has monitored the average of measured visible radiances (converted to narrowband albedo using an empirical bidirectional model for deserts) over the Libyan desert obtained from NOAA-6, NOAA-7 and NOAA-9. Figure 15 shows a comparison of his inferred albedos to our reflectances for NOAA-9. Despite the different treatments of angle dependence (our neglect of solar zenith angle dependence in the monitoring procedure causes the small seasonal oscillation in our results), the agreement is excellent: calculated trends are the same to a precision better than 1 per cent.

A cooperative effort is underway to intercompare calibration methods for AVHRR solar channels and to obtain a best value for the absolute calibrations (Whitlock *et al.* 1990). The comparison of six different sets of measurements (including the Staylor results) provides additional confirmation of the trend inferred for NOAA-9 Channel 1. Trends inferred from the point measurements representing independent calibra-

tions at different times, using models, known sites and coincident aircraft measurements, agree well with the two (ISCCP and Staylor's) satellite methods.

We can verify our normalization of NOAA-9 to NOAA-7 by comparison to Staylor's (1990) normalization: he cites a normalization factor of 0.935, which differs from our value of 0.835 (+0.2 per cent). However, this is due to a difference in normalization procedures. We normalize to the performance of NOAA-7 in January 1985, assumed to be nearly the same as that in July 1983. Staylor normalizes to NOAA-7 data corrected for its degradation since launch. If we apply his NOAA-7 degradation model through January 1985 and recompute his normalization factor accordingly, we get a value of 0.823 which compares very well with our value of 0.835 (+0.2 per cent).

6.4. *Absolute calibration of AVHRR*

The results of an intercomparison of several absolute and relative calibration methods for NOAA-9, combined with the absolute measurements obtained from simultaneous and coincident aircraft measurements (from the NASA ER-2 collected in October 1986), provides an absolute calibration for AVHRR Channel 1 (Channel 2 was also calibrated) (Whitlock *et al.* 1990). This value is much more accurate than that originally adopted for ISCCP, which was based on the qualitative agreement of measured vegetation reflectances with literature values. Consequently, this new absolute calibration is applied to all ISCCP visible data before an analysis using a radiative transfer model to obtain cloud and surface properties (Rossow *et al.* 1988).

The correction to the original visible calibration recorded on all ISCCP (B3) radiance data tapes is to multiply by 1.2. This illustrates a key attribute of the ISCCP data: since the original count values are reported on the data tapes, together with the original calibration supplied by the satellite operator, as well as any corrections performed by us to normalize to the ISCCP reference standard, users can not only re-examine these calibration adjustments, but also exploit any new information obtained after the tapes were produced. Thus, we easily incorporated this absolute calibration into the cloud climatology analysis by introducing the correction at the beginning of the analysis software.

Further work is underway to understand these results better, to add more aircraft flights, and to attempt to compare this calibration to that of the broadband instruments on ERBE and NIMBUS-7. When completed, we will have, for the first time a well established, well defined absolute calibration for satellite measurements at solar wavelengths. Some studies are also underway to intercompare IR calibrations as well.

To repeat, the recommended visible channel calibration, used by ISCCP for the cloud analysis, is 1.2 times the radiance values obtained from ISCCP B3 tapes using the ‘absolute’ calibration tables.

6.5. *ISCCP AVHRR absolute calibrations*

As stated in §1.2.2 the scaled radiance (per cent) can be obtained from count values using:

$$L_1^* = G_1(CT_8) + Y_1$$

Here we present the appropriate values for all three satellites for users of B3 data. Users of AVHRR 10-bit data can make the appropriate conversion by dividing the

gain by 4.0 (see below for illustration). These calibrations include all ISCCP normalizations, trend corrections, and the absolute aircraft calibration.

For NOAA-7 the calibration from July 1983 to January 1985 is

$$L_1^* = 0.5126\,(CT_8) - 4.128 \qquad \text{[NOAA-7 absolute]}$$

(If we were to correct for the apparent trend (0.7 per cent over 19 months), then in January 1985 the calibration equation would be $L_1^* = 0.5126(CT_8) - 4.157$.)

For NOAA-8 the calibration from October 1983 to June 1984 is

$$L_1^* = 0.5090\,(CT_8) - 4.994 \qquad \text{[NOAA-8 absolute]}$$

For NOAA-7 and NOAA-8 there is only one calibration because there is no normalization or trend correction necessary.

For NOAA-9 the calibration varies monthly because of the trend correction. We show each of the steps in deriving the final set of calibrations for NOAA-9. For NOAA-9 the nominal calibration is given by

$$L_1^* = 0.4254\,(CT_8) - 3.846 \qquad \text{[NOAA-9 nominal]}$$

Next we incorporate the normalization factors

$$L_1^* = 0.3522\,(CT_8) - 3.213 \qquad \text{[NOAA-9 normalized]}$$

We still have to incorporate the correction for sensor degradation (the ISCCP absolute calibration) and the 1.2 correction factor derived from the ER-2 aircraft calibration field program in October 1986. We illustrate the application of these using the last month of data. Starting with the normalized calibration equation, we apply the absolute calibration correction (for November 1988 the monthly absolute correction is 1.177). Applying this to the normalized equation yields

$$L_1^* = 0.4181\,(CT_8) - 3.782 \qquad \text{[NOAA-9 Nov. 1988 ISCCP absolute]}$$

and applying the 1.2 aircraft correction

$$L_1^* = 0.5017\,(CT_8) - 4.538 \qquad \text{[NOAA-9 Nov. 1988 absolute]}$$

In general, the absolute calibration for NOAA-9 data is given by

$$L_1^* = G_1\,(CT_8) + Y_1 \qquad \text{[NOAA-9 absolute]}$$

where G_1 and Y_1 are obtained from table 5 for the appropriate month from February 1985 to November 1988. These values represent our best effort at calibration.

There is a slight difference between the preliminary calibration (used by ISCCP) and the final calibration from the October 1986 aircraft calibration field program (Whitlock *et al.* 1990). Because of this we want to compare them to verify that this difference will not have a significant effects on our results. We first convert our calibration for October 1986

$$L_1^* = 0.4582\,(CT_8) - 4.145$$

to that for 10-bit data

$$L_1^* = 0.1146\,(CT_{10}) - 4.145$$

Next we convert from scaled radiance (L^*) to radiance (L) by multiplying by $E_{o1}/100$ (see §1.2.2), using a value of $E_{o1} = 519.4$ from Whitlock *et al.* (1990). This yields

$$L_1^* = 0.5952\,(CT_{10}) - 21.5$$

Comparing this equation with the final result from Whitlock *et al.*, which has an estimated uncertainty of ±5 per cent:

$$L_1^* = 0.6060\,(CT_{10}) - 22$$

indicates agreement to within 1 per cent.

Several remarks can be made about the difference. The exact date used in the calculation can be significant. We use the midpoint of each month and the difference in gain between this day and the first (or last) day of the month can be almost 1 per cent. The solar constant used by Whitlock *et al.* differs slightly from the ISCCP value

Table 5. Absolute calibration coefficients for NOAA9, Channel 1.

Month	G_1 (gain)	Y_1 (offset)
February 1985	0.4262	3.856
March 1985	0.4279	3.871
April 1985	0.4292	3.883
May 1985	0.4309	3.898
June 1985	0.4326	3.913
July 1985	0.4339	3.925
August 1985	0.4356	3.940
September 1985	0.4373	3.956
October 1985	0.4386	3.967
November 1985	0.4403	3.983
December 1985	0.4420	3.998
January 1986	0.4437	4.014
February 1986	0.4450	4.025
March 1986	0.4467	4.041
April 1986	0.4484	4.056
May 1986	0.4501	4.072
June 1986	0.4518	4.087
July 1986	0.4531	4.099
August 1986	0.4548	4.114
September 1986	0.4565	4.129
October 1986	0.4582	4.145
November 1986	0.4599	4.160
December 1986	0.4616	4.176
January 1987	0.4633	4.191
February 1987	0.4650	4.206
March 1987	0.4667	4.222
April 1987	0.4684	4.237
May 1987	0.4701	4.253
June 1987	0.4718	4.268
July 1987	0.4736	4.284
August 1987	0.4753	4.299
September 1987	0.4770	4.314
October 1987	0.4787	4.330
November 1987	0.4804	4.345
December 1987	0.4821	4.361
January 1988	0.4838	4.376
February 1988	0.4855	4.392
March 1988	0.4872	4.407
April 1988	0.4889	4.422
May 1988	0.4906	4.438
June 1988	0.4927	4.457
July 1988	0.4944	4.472
August 1988	0.4961	4.488
September 1988	0.4978	4.503
October 1988	0.4996	4.519
November 1988	0.5017	4.538

(Rossow *et al*. 1987), but this would change the results by only a few tenths of a per cent.

Having anchored our relative calibration using the October 1986 aircraft observations, we can validate our trend for NOAA-9 by comparing our calibration to that of another aircraft field program flown in November 1988 (Guenther 1990) during the last month of NOAA-9 data

$$L_1 = 0.6513\ (CT_{10}) - 23.4 \qquad \text{[ISCCP]}$$
$$L_1 = 0.6410\ (CT_{10}) - 24.4 \qquad \text{[Guenther]}$$

These agree to within 2 per cent. The current estimated uncertainty of the last aircraft value is ±6 per cent. The excellent agreement between the ISCCP calibration and these absolute calibration field programmes indicates that the ISCCP calibration accurately characterizes the behavior of the NOAA AVHRR Channel 1 data from July 1983 through November 1988.

6.6. *Status and plans*

The ISCCP analysis has now been applied to the normalization of the VIS (≈ 0.6 μm) and IR (≈ 11 μm) channels for the following satellites for the time period from July 1983 through 1988: NOAA-7, NOAA-8, NOAA-9, GOES-5, GOES-6, GMS-1, GMS-2, GMS-3, and METEOSAT-2. During the next year the time period covered will be extended and the normalization will be applied to NOAA-10, NOAA-11, GOES-7, GMS-4, METEOSAT-3, and METEOSAT-4. This analysis will continue throughout the ISCCP, which is currently planned to continue through 1995. We may be able to use the Staylor's results to extend the NOAA-7 results back to 1981 and to transfer the normalization to NOAA-6. The results of Frouin and Gautier (1987) may be used to extend these results to GOES-4, while the results of Kriebel (1981) can be used to extend them METEOSAT-1.

Acknowledgments

We gratefully acknowledge support for this research provided by the NASA Climat Program managed by Robert Schiffer. We would also like to thank C. Whitlock, W. F. Staylor, J. C. Price and C. J. Justus for discussions of satellite calibration, and Lilly Del Valle for drawing the figures.

Appendix: Thermal IR calibration history

Calibration of the infrared channels is carried out actively on the spacecraft, once per scan, by having the radiometer view space and a standard black-body with a known temperature (Kidwell 1988, Rossow *et al.* 1987). Operational production of sea surface temperature data sets from AVHRR and their comparisons to ship measurements presumably maintain the overall calibration. Pre-launch measurements of a precision calibration black-body with the radiometer are used to relate the output counts from four thermistors to the temperature of the reference black-body with a fourth-order polynomial. This temperature is converted to a radiance by integrating the product of the Planck function and the spectral response functions (see Rossow *et al.* 1987, §7.2). NOAA documentation provides calibration in terms of radiance per unit wavelength J, i.e. $L = JB$, where B is the radiometer bandwidth. From the spec-

tral response functions for Channel 4, bandwidths are calculated to be $B_4 = 73.06$ cm^{-1} for NOAA-7, $B_4 = 69.64$ cm^{-1} for NOAA-8, and $B_4 = 73.96$ cm^{-1} for NOAA-9.

The radiometer counts for measurements of space CT_{sp} and the on-board black-body CT_{bb} are used to calibrate the radiometer by calculating a gain G_4 and intercept Y_4 (Kidwell 1988, Lauritson *et al.* 1979).

$$G_4 = (J^4_{sp} - J^4_{bb})(CT^4_{sp} - CT^4_{bb})^{-1}$$
$$Y_4 = J^4_{sp} - G(CT^4_{sp})$$

J^4_{bb} is the reference black-body radiance calculated from its measured temperature and J^4_{sp} is the radiance of space, adjusted to account for slight non-linearity in the radiometer response. For NOAA-7, $J^4_{sp} = -1.176$ mWm^{-2}sr^{-1}cm. Sample values of G_i and Y_i are $G_4 = -0.62141$ and $Y_4 = 152.93695$ mWm^{-2}sr^{-1}cm. For NOAA-8, $J^4_{sp} = -2.784$ mWm^{-2}sr^{-1}cm. Sample values of G_i and Y_i are $G_4 = -0.6527$ and $Y_4 = 159.2977$ mWm^{-2}sr^{-1}cm. For NOAA-9, $J^4_{sp} = -3.384$ mWm^{-2}sr^{-1}cm. Sample values of G_i and Y_i are $G_4 = -0.64130$ and $Y_4 = 155.09058$ mWm^{-2}sr^{-1}cm.

Radiance measurements can be converted to brightness temperatures by inverting the relation

$$L_i = \int B(v, T)\, \phi_i(v)\, dv$$

where $B(v, T)$ is the Planck function of temperature and frequency, v is in units of cm^{-1}, and $\phi_i(v)$ is the normalized spectral response of the radiometer. An approximate relation, equivalent to the above for three temperature ranges, is given by Kidwell (1988).

$$TB(J_i) = C_2 \bar{v}_i \{ln[1 + C_1 \bar{v}^3_i (J_i)^{-1}]\}^{-1}$$

where $C_i = 1.1910659 \times 10^{-5}$ mWm^{-2}sr^{-1}cm^4; $C_2 = 1.438833$ cmK, and $\bar{v}_i$ represents an effective frequency of the radiometer for a specific temperature range.

On ISCCP radiance data tapes, the calibration coefficients (G_i and Y_i) for the firs scan line in an orbit swath are used for all scan lines in that orbit. Since the calibration actually changes somewhat during the orbit (owing to varying thermal environment), the count values are altered so that constant coefficients reproduce the original data. For Channel 4 the changes in calibration are no more that 2-3 per cent, occurring primarily when the satellite passes from the night to dayside of the Earth; consequently only the lowest count values actually change.

Figure 16 shows the history of Channel 4 (thermal infrared) calibration for NOAA-7 and NOAA-9 as the global and monthly mean value of counts from the AVHRR brightness temperature and the inferred on-board calibration. Each point represents an average of all the data collected by ISCCP for that month. We assume that the global, annual mean temperature of the Earth is also constant over time periods of 5-10 years. None of the calibration standards is more accurate than 1-2 K (e.g. Njoku 1985). The evolution on global monthly mean temperatures shown in figure 16 exhibits a seasonal variation, but no trend, over 4-5 years. The average count values suggest that the NOAA-9 channel sensitivity changed slowly with time an differed significantly from that of the NOAA-7 channel; however, the calibration procedure has eliminated these variations. The initial difference in calibration between NOAA-7 and NOAA-9 (figure 16) is similar in magnitude to differences between coincident observations by NOAA-7 and NOAA-8 (table 6). We have also examined

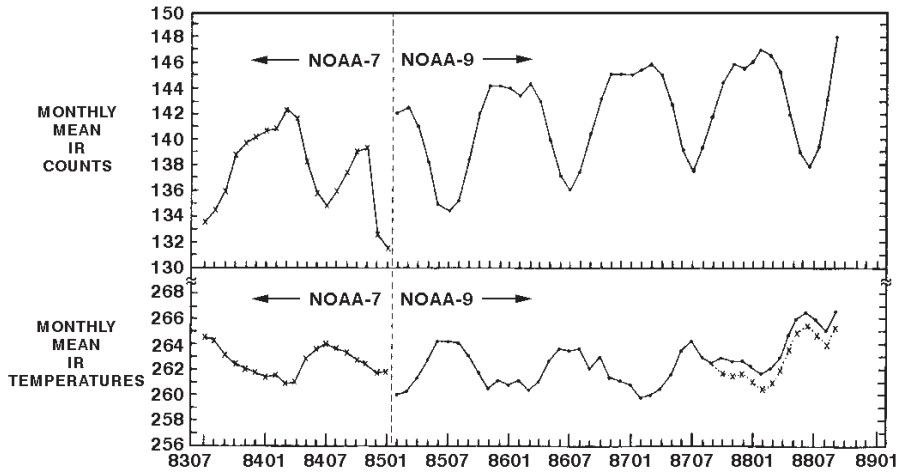

Figure 16. Time history of AVHRR Channel 4 calibration for NOAA-9, shown as monthly global mean counts and temperature values. The differences between the two radiometers and the drift of the NOAA-9 radiometer, as shown by the mean count values, are eliminated in the operational calibration procedure that uses an on-board standard source.

Table 6. Model differences of IR radiances

8310†	8311	8312	8401	8402	8403	8404	8405
1.0	0.5	0.5	1.5	1.0	1.5	0.5	0.5

Difference between NOAA-7 and NOAA-8 are expressed as brightness temperatures. Observations are averaged over co-located regions approximately 250 km across and are compared if they occur within 3 hours of each other. Distributions of radiance differences are collected for the whole month.

† In the form of YYMM representing year and month; for example 8310 is October 1983.

this same time record on a daily basis and find only one significant short-term calibration anomaly. This anomaly is also revealed as an apparent coherent change in the IR calibration of GOES-6, GOES-7, GMS-3 and Meteosat-2. The dotted line (figure 16) illustrates the corrected calibration, obtained by multiplication by 1.038 and an offset −11.5K. This change affected the colder brightness temperatures primarily. We conclude that the calibrations of the IR (Channel 4) measurements are generally stable to within about 1K.

These results, together with the geostationary satellite normalization (for both the

visible ad thermal infrared channels) performed by the ISCCP Satellite Calibration Centre (Centre de Meteorologie Spatial, Lannion, France), provide a uniform calibration for GOES-5, 6 and 7, GMS-1, 2 and 3, and METEOSAT-2 and 3.

References

AHERN, J., GOODENOUGH, D. G., JAIN, S. C., and RAO, U. P., 1977, Use of clear lakes as standard reflectors for Atmospheric measurements. In *Proceedings of the Eleventh International Symposium, on Remote Sensing of Environment held in Ann Arbor, Michigan* (Environmental Research Institute of Michigan), **11**, 731-55.

BREST, C. L., 1987, Seasonal albedo of an urban/rural landscape from satellite observations. *Journal of Climate and Applied Meteorology*, **26**, 1169-1187.

BREST, C. L., and GOWARD, S. N., 1987, Deriving surface albedo from narrow band satellite data. *International Journal of Remote Sensing*, **8**, 351-367.

CASTLE, K., HOL, R., KASTNER, C., PALMER, J., SLATER, P., DINGUIRART, M., EZRA, C., JACKSON,R., and SAVAGE, R., 1984, In-flight absolute radiometric calibration of the Thematic Mapper. *I.E.E.E. Transactions on Geoscience and Remote Sensing*, **22**, 251-255.

COAKLEY, J. A., and BRETHERTON, F. P., 1982, Cloud cover from high-resolution scanner data: Detecting and allowing for partially filled fields of view. *Journal of Geophysical Research*, **87**, 4917-4932.

DESBOIS, M, SEZE, G., and SZEJWACH, G., 1982, Automatic classification of clouds on METEOSAT imagery: Application to high-level clouds. *Journal of Applied Meteorology*, **21**, 401-412.

EATON, F. D., and DIRMHIRN, I., 1979, Reflected irradiance indicatrices of natural surfaces and their effect on albedo. *Applied Optics*, **18**, 994-1008.

FROUIN, R., and GAUTIER, C., 1987, Calibration of NOAA-7 AVHRR, GOES-5, and GOES-6 VISSR/VAS solar channels. *Remote Sensing of Environment*, **22**, 73-102.

GUTMAN, G., 1987, The derivation of vegetation indices from AVHRR data. *International Journal of Remote Sensing*, **8**, 1235-1243.

GUTMAN, G., TARPLEY, D., and OHRING, G., 1987, Cloud screening for determination of land surface characteristics in a reduced resolution satellite data set. *International Journal of Remote Sensing*, **8**, 859-870.

HILSENRATH, E., and SCHLESINGER, B. M., 1981, Total ozone seasonal and interannual variations derived from the 7 year NIMBUS-4BUV data set. *Journal of Geophysical Research*, **86**, 12087-12096.

HOLBEN, B., KIMES, D. S., and FRASER, R. S., 1986, Directional reflectance response in AVHRR red and near-IR bands for three cover types and varying atmospheric conditions. *Remote Sensing of Environment*, **19**, 213-236.

HOVIS, W. A., KNOLL, J. S., and SMITH, G. R., 1985, Aircraft measurements for calibration of an orbiting spacecraft sensor. *Applied Optics*, **24**, 407-410.

INN, E. C. Y., and TANAKA, Y., 1953, Absorption coefficient of ozone in the ultraviolet and visible regions. *Journal of the Optical Society of America*, **43**, 870-873.

KIDWELL, K. B., 1988, *NOAA Polar Orbiter Data Users Guide* (Washington, D. C.: National Oceanic and Atmospheric Administration).

KIMES, D. S., 1983, Dynamics of directional reflectance factor distributions for vegetation canopies. *Applied Optics*, **22**, 1364-1372.

KIMES, D. S., and KIRCHNER, J. A., 1983, Diurnal variations of vegetation canopy structure. *International Journal of Remote Sensing*, **4**, 257-271.

KIMES, D. S., and SELLERS, P. J., 1985, Inferring hemispherical reflectance of the Earth's surface for global energy budgets from remotely sensed nadir or directional radiance values. *Remote Sensing of Environment*, **18**, 205-223.

KOEPKE, P., 1982, Vicarious satellite calibration in the solar spectral range by means of calculated radiances and its application to METEOSAT. *Applied Optics*, **21,** 2845-2854.

KOWALIK, W. S., MARSH, S. E., and LYON, R. P. J., 1982, A relation between Landsat digital numbers, surface reflectance, and the cosine of the solar zenith angle. *Remote Sensing of Environment*, **12**, 39-55.

KRIEBEL, K. T., 1979, Albedo of vegetated surfaces: Its variability with differing irradiances. *Remote Sensing of Environment,* **8**, 283-290.

KRIEBEL, K. T., 1981, Calibration of the METEOSAT-VIS channel by airborne measurements. *Applied Optics,* **20**, 11-12.

LACIS, A. A., and HANSEN, J. E., 1974, A parameterization for the absorption of solar radiations in the Earth's atmosphere. *Journal of Atmospheric Science,* **31**, 118-133.

LAURITSON, L., NELSON, G. J., and PORTO, F. W., 1979, Data extraction and calibration of TIROS-N/NOAA radiometers. *NOAA Technical Memo NESS 107*, National Oceanic and Atmospheric Administration, US. Dept. Of Commerce.

LYON, R. J. P., HONEY, F. R., and BALLEW, G. I., 1975, A comparison of observed and model-predicted atmospheric perturbations on target radiances measured by ERTS: Part I-Observed data and Analysis. *Proceedings of the Institute of Electrical and Electronic Engineers,* **75,** 244-249.

MATTHEWS, E., 1983, Global vegetation and land use: New high resolution data bases for climate studies. *Journal of Climate and Applied Meteorology,* **22**, 474-487.

MATTHEWS, E., 1984, Vegetation, land use, and albedo data sets: Documentation of archived data sets. *NASA TechnicalMemo 86107,* Washington, D.C.

MATTHEWS, E. and ROSSOW, W. B., 1987, Regional and seasonal variations of surface reflectance from satellite observations at 0.6 μ. *Journal of Climate and Applied Meteorology,* **26**, 170-202.

NASA, 1984, Earth observing system: science and mission requirements working group report, Vol. 5. NASA Technical Memo 86129, Washington, D.C.

NECKEL, J., and LABS, D., 1984, The solar radiation between 3300 and 12500 Å. *Solar Physics,* **90**, 205-258.

NELSON, R. F., 1985, Sensor-induced temporal variability of Landsat MSS data. *Remote Sensing of Environment,* **18**, 35-48.

NJOKU, E. G., 1985, Satellite-derived sea surface temperature: Workshop comparisons. *Bulletin of the American Meteorology Society, **66,*** 274-281.

PRICE, J. C., 1984, Radiometric calibration of satellite sensors in the visible and near infrared: history and outlook. *Remote Sensing of Environment,* **22**, 3-9.

ROBINOVE, C. J., 1982, Computation with physical values from Landsat digital data. *Photogrammetric Engineering and Remote Sensing,* **48**, 781-784.

ROSSOW, W. B., KINSELLA, E., WOLF, A., and GARDER, L. C., 1987, International Satellite Cloud Climatology Project (ISCCP) Description of reduced resolution radiance data. World Climate Research Programme. *World Meteorological Organization Technical Document No. 58.*

ROSSOW, W. B., GARDER, L. C., LU, P. J., and WALKER A. W., 1988, International Satellite Cloud Climatology Project (ISCCP) Documentation of cloud data. World Climate Research Programme. *World Meteorological Organization Technical Document No. 266.*

ROSSOW, W. B., BREST, C. L., and GARDER, L. C., 1989 a, Global, seasonal surface variations from satellite radiance measurements. *Journal of Climate,* **2**, 214-247.

ROSSOW, W. B., GARDER, L. C., and LACIS A. A., 1989 b, Global, seasonal cloud variations from satellite radiance measurements. 1: Sensitivity of analysis. *Journal of Climate,* **2**, 423-462.

SCHIFFER, R. A., and ROSSOW, W. B., 1985, ISCCP global radiance data set: A new resource for climate research. *Bulletin of the American Meteorology Society,* **66**, 1498-1505.

SEZE, G., and ROSSOW, W. B., 1991, Time-cumulated visible and infrared radiance histograms used as descriptors of surface and cloud variations. *International Journal of Remote Sensing,* to be published.

SLATER, P. N., BIGGAR, S. F., HOLM, R. G., JACKSON, R. D., MAO, Y., MORAN, M. S., PALMER, J. M., and YUAN, B., 1987, Reflectance and radiance-based methods for the in-flight absolute calibration of multispectral sensors. *Remote Sensing of Environment,* **22**, 11-38.

STAYLOR, W. F., 1990, Degradation rates of the AVHRR visible channel for the NOAA-6, 7 and 9 spacecraft. *Journal of Atmospheric and Oceanic Technology*, **7,** 411-423.

WHITLOCK, C. H., PURGOLD, G. C., and LECROY, S. R., 1987, Surface bidirectional reflectance properties of two southwestern Arizona deserts for wavelengths between 0.4 and 2.2

micrometers. *NASA Technical Paper 2643*, Washington, D.C.

WHITLOCK, C. H., STAYLOR, W. F., SMITH, G., LEVIN, R., FROUIN, R., GAUTIER, C., TEILLET, P. M., SLATER, P. N., KAUFMAN, Y. J., HOLBEN, B. N., ROSSOW, W. B., BREST, C. L., and LECROY, S. R., 1990, AVHRR and VISSR satellite instrument calibration results for both Cirrus and Marine Stratus IFO periods, FIRE Science Report 1988, *NASA Conference Proceedings 3083* (Washington, D. C.: NASA).